Land use~~Land-surface forcing~~ and anthropogenic heat modulate ozone by meteorology: A perspective from the Yangtze River Delta region

Chenchao Zhan [a], Min Xie [a,*]

[a] School of Atmospheric Sciences, CMA-NJU Joint Laboratory for Climate Prediction Studies, Jiangsu Collaborative Innovation Center for Climate Change, Joint Center for Atmospheric Radar Research of CMA/NJU, Nanjing University, Nanjing 210023, China

----

[*] Corresponding author. minxie@nju.edu.cn (M. Xie)

Abstract: With the rapid advance in urbanization, ~~-land-surface forcing related to the~~ land use~~urban expansion~~ and anthropogenic heat (AH) ~~release from human activities~~dictated by human activities significantly modify ~~affect~~ the urban climate and in turn the air quality. Focusing on the Yangtze River Delta (YRD) region, a highly urbanized coastal area with sever ozone (O_3) pollution ~~a highly urbanized place with sever ozone (O_3) pollution and complex geography~~, we estimate the impacts of~~-~~ land use~~land-surface forcing~~ and AH on meteorology ~~(meteorological factors and local circulations)~~ and O_3 using the WRF-~~chem~~ Chem model, ~~;~~ which can enhance our understanding about the formation of O_3 pollution in those rapidly developing ~~regions~~ city clusters with ~~unique geographical features~~place-specific topography as most of our results can be supported by previous studies conducted in other regions around~~in~~ the world. Regional O_3 pollution episodes occur frequently (~26 times per year) in the YRD in recent years. These O_3 pollution episodes are usually in~~under~~ calm conditions characterized by high temperature (over 20 °C), low relative humidity (less than 80%), light wind (less than 3 m s^{-1}) and shallow cloud cover (less than 5 okta). In this case, ~~In this case, high O_3 mainly appears during the daytime influenced by~~O_3 pollution belts tend to appear in the converging airflows associated with the ~~local circulations (the~~ sea and the ~~the~~ lake breezes~~s)~~. The fast urbanization has significantly changed land use and AH in this region. The largest change in land use comes from the urban expansion, which~~The change in land-surface forcing can~~ causes an increase in 2-m temperature (T_2) by maximum 3 °C, an increase in planetary boundary layer

height (PBLH) by maximum 500 m, and a decrease in 10-m wind speed (WS_{10}) by maximum 1.5 m s^{-1}, and an increase in surface O_3 can increase by maximum 20 μg m^{-3} eventually. With regard to the sea and lake breezesFurthermore, the expansion of coastal cities, like Shanghai, can enhancess the sea-breeze below 500 mthe sea breeze circulation by ~1 m s^{-1}. During the advance of the sea -breeze front inland, the upward air flowupdraft induced by the front makes well vertical mixing of O_3. However, once the sea -breeze is fully-developedfully formed at afternoon (~17:00 LT), further progression inland will beis stalled. Then, thus the O_3 removal by the low sea -breeze will be weakened and surface O_3 can be 10 μg m^{-3} higher in the case with cities than no-cities. The expansion of lakeside cities, like Wuxi and Suzhou, can extend the lifetime of the lake -breeze from the noon to the afternoon. Since the net effect of the lake-breeze is to accelerate the vertical mixing in the boundary layerthe offshore flow of the lake breeze transports high O_3 from the land to the lake, the onshore flow brings the high O_3 back to the land. the SSurface O_3 in lakeside cities can increase as much as 30 μg m^{-3} in lakeside cities. Compared towith the effects from land-surface forcingland use, the effect impacts of AH are relatively small. And the changes mainly appear in and around cities where AH emission fluxes areis large. There are increases in T_2, PBLH, WS_{10} and surface O_3 when AH are taken into account, with the increment ofabout about 0.2 °C, 75 m, 0.3 m s^{-1} and 4 μg m^{-3}, respectively. Additionally, AH can affect the urban-breeze circulations, meteorological factors and O_3 concentrationcontributes largely to the urban environment, altering meteorological factors, O_3 concentration and urban breeze circulation, but its effect on local circulations, such as the sea and the lake breezes, seems to be limited.

Key Words: ozone; meteorology; local circulations; land-surface forcingland use; anthropogenic heat; the Yangtze River Delta;

1 Introduction

Ozone (O_3) is a key constituent in the atmosphere, and is deeply relevant to climate (Worden et al., 2008), biosphere (Van Dingenen et al., 2009) and human health (Jerrett et al., 2009). O_3but acts quite differently in different parts of the atmosphere, often described as being "good up high and bad nearby". O_3 in the stratosphere helps protect life on earth from strong ultraviolet radiation. However, high O_3 in the troposphere is harmful to human respiratory system (Jerrett et al., 2009), and the growth of vegetation (Mills et al., 2011) and climate (Worden et al., 2008)., and

Therefore,thereby the tropospheric O_3 has long been regarded as an important air pollutant and has received continuous attention within the last few decades(Young et al., 2013).

Tropospheric O_3 is a secondary air pollutant, which is mainly formed by a series of complex chemical reactions (Chameides and Walker, 1973; Xie et al., 2014) of precursor gases such as nitrogen oxides (NO_x=NO+NO_2) and volatile organic compounds (VOCs) in combination with sunlight. The global average lifetime of tropospheric O_3 is 20 to 25 days, and it will be reducedreduce to 5 days in boundary layer (Young et al., 2013). The relatively long lifetime of tropospheric O_3 favors regional/long-range transport, and brings huge challenges to its control (Shao et al., 2006Bergin et al., 2005). O_3 levels considerably depend on the variations in weather conditions because theyweather conditions play an important role in determining the chemistry, dispersion and removal of O_3 (Jacob and Winner, 2009). GenerallyIn general, elevated O_3 occurs under warm dry weather with strong sunlight, high temperature, low relative humidity and light wind speed (Zhang et al., 2015). Furthermore, weather conditions can have many similarities in certain weather pattern (Buchholz et al., 2010; Zhan et al., 2019), and the main weather patterns associated with O_3 episodes in China are tropical cyclones and continental anticyclones (Wang et al., 2017).

O_3 levels concentrations as well as weather conditionsmeteorology in urban areas are of great concern simply because urban areas have huge populations. A report from the United Nations pointed out that 69.6% of the world's population will live in cities by 2050. The urbanization process has alsofurther increased urban environmental hazards (Zhang et al., 2011), particularly in the most rapidly developing countries like China (Liu and Tian, 2010). Because of historical and cultural factors, many cities have similar topography, usually along the coast, close to mountains or in basins. For these cities, the local circulations induced by thermal contrast of the topography, such as sea-land breezes, mountain-valley breezes and lake-land breezes, will have an important impact on urban air quality of the city, especially under weak synoptic forcingwhen the dominant background weather system is weak (Crosman and Horel, 2010). Examples can be found around the world. Ding et al. (2004) simulated the main features of the sea-land breezes during a multiday episode in the Pearl River Delta (PRD) region, and found that the sea-land breezes can play a crucial role in transport ing air pollutants between inland and coastal cities. Miao et al. (2015) studied the effects of mountain-valley breezes on boundary layer structure in the Beijing-Tianjin-Hebei (BTH) region, suggesting that the mountain-valley breezes are vital to the vertical transport and distribution of air pollutants in Beijing. Wentworth et al. (2015) identified a causal link between lake ~~-~~breezes and O_3 in the Greater Toronto Area that the daytime O_3 maxima was 13.6-14.8 ppb higher on lake breeze days than no-lake breeze days.

~~The land-surface forcing and anthropogenic heat (AH) of a city also affect the atmospheric state and compositions above it~~Human activities, such as changes in land use and anthropogenic heat (AH), contribute to changes of meteorology and atmospheric compositions at local, regional and even global scales (Fu and Liao, 2014~~Yu et al., 2012~~; Park et al., 2014; Oke et al., 2017). ~~The land-surface forcing~~Land use changes via urban expansion (typically from vegetation to impervious surface)~~- changes chiefly come from the urban expansion (typically from vegetation to impervious surface), which~~ directly alters~~changes~~ the surface physical properties (e.g., albedo, surface moisture and roughness), subsequently affecting the exchange of energy, moisture and momentum, and hence impacting the urban climate and air quality (Jiang et al., 2008; Wang et al., 2009) ~~and thereby significantly affects the meteorology and in turn the air quality~~. Li et al. (2019) found that increases in thermal inertia, surface roughness and evapotranspiration due to urban expansion can ~~can lead to an increase in~~rise O_3 by ~~up to~~ 5.6 ppb in Southern California. AH is an important waste by-product of urban metabolism. Nearly all energy consumed by human activities will be dissipated as heat within Earth's land-atmosphere system (Flanner, 2009; Sailor, 2011) that is then "injected" into the energy balance processes. Ryu et al. (2013a) reported that AH affects the characteristics/structures of boundary layer and local circulations, resulting in an increase of O_3 by 3.8 ppb in the Seoul metropolitan area.

~~These p~~Previous studies ~~separately~~usually investigated the impact of ~~local circulations~~topography, land use~~, land-surface forcing~~ and AH on meteorology and ~~and~~ air quality ~~,~~ separately, and mainly~~usually~~ focusing on a specific megacity. However, ~~local circulations, land-surface forcing and AH~~these factors can work together in near-calm conditions. Furthermore, complex interactions exist widely among these thermally-driven circulations and the effects can even spread from one city to nearby areas. For example, Zhu et al. (2015) demonstrated that the meteorological conditions and air quality over Kunshan are significantly affected by Shanghai urban land surface forcing (Kunshan is located downstream of Shanghai, with a straight-line distance of about 50 km). Given the increasing prevalence of cities, cities gradually appear in the form of clusters. Therefore,And the role of multi-scale atmospheric circulations associated with the abovementioned factors in regional meteorology and air quality of city clusters is unclear. Actually, complex interactions exist widely among these thermally-driven circulations and the effects can even spread from one city to nearby areas. For example, Zhu et al. (2015) demonstrated that the meteorological conditions and air quality over Kunshan are significantly affected by Shanghai urban land surface forcing (Kunshan is located downstream of Shanghai, with a straight-line distance of about 50 km). Therefore, assessing the effects of land-surface forcingland use –and AH (tThe topography rarely changes.) in the city cluster is meaningful, which helps understand the interactionsconnection between urban environment and human activities development, local meteorology and regional air quality.

The Yangtze River Delta (Yangtze River Delta (YRD)) region, located on the western coast of the Pacific Ocean (Figure 1a), has undergone accelerated urbanization process and rapid economic development over the the past few decades, and. It is now one of the largest economic zones in the world. The YRD regionIt includes the areas ofconsists of the southern part of Jiangsu Province, the northern part of Zhejiang Province and the eastern part of Anhui Province, includingwith 26 mega/large cities such as Shanghai, Hangzhou and Nanjing (Figure 1b). With dense population and huge energy consumption, this area is now suffering from air quality deterioration (Ding et al., 2013; Xie et al., 2017; Zhan et al., 2020), especially the increasingly severe O_3 pollution in recent years (Li et al., 2020; Wang et al., 2020Zhan et al., 2020, 2021). Furthermore, It was reported that 16 out of the 26 typical cities in the YRD failed to meet the urban national standard for O_3 in 2017 (Bulletin on the state of China's ecological environment in 2018, http://www.cleanairchina.org/product/9943.html), and to make matters worse, O_3 concentration has been rising in this region during the past few years (Li et al., 2020; Wang et al., 2020). The YRD region is deeply affected by the East Asian monsoon, and has complex weather like other mid-latitude regions in the worldcities with hot spots of O_3 usually concentrate in the central YRD region, surrounding Tai Lake (Zhan et al., 2021). Numerous cities, unique topography and s. Sever O_3air pollution and unique geography make this areahe YRD an ideal study place for studying the .complex interactions between the atmosphere and human activities.

In this study, the impacts of land-surface forcingland use and AH on meteorology in the central YRD region, and how these impacts further modulate O_3 are investigated using the Weather

Research and Forecasting model coupled to Chemistry (WRF-Chem). These results fill the knowledge gap about the formation of O_3 pollution in this region and provide valuable insight for other rapidly developing regions with complex ~~geography~~topography in the world. The remainder of this paper is organized as follows. Sect. 2 gives a detailed description about the observation data, the model setup and experimental design. The main results, including the characteristics of O_3 pollution episodes, the model evaluation and the changes in meteorology and ~~response of~~ O_3 caused by~~to~~ ~~land-surface forcing~~land use and AH, are presented in Sect. 3. Summary and conclusions are given in Sect. 4.

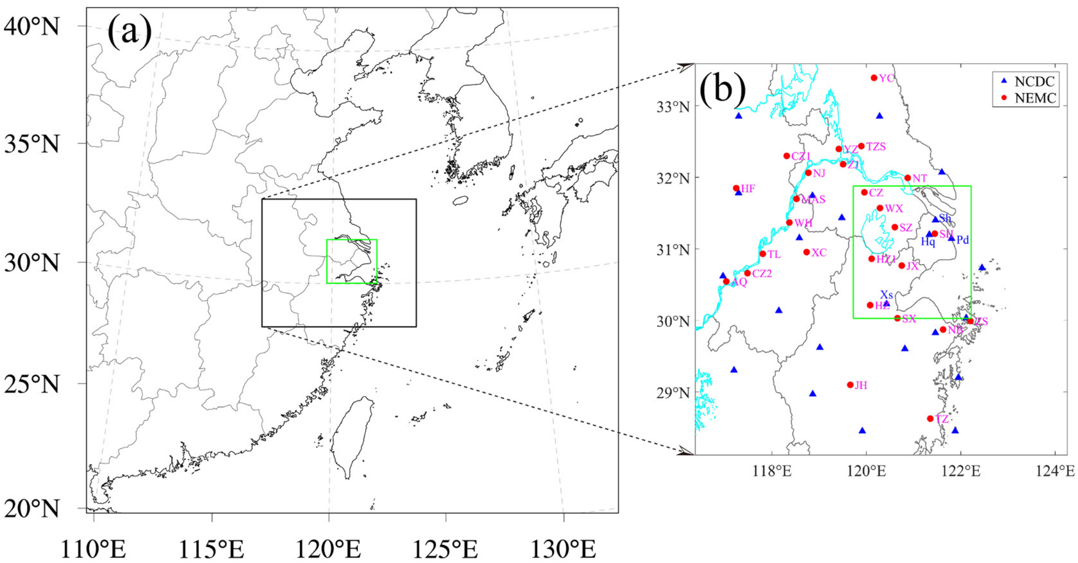

Figure 1. (a) Three nested WRF-Chem domains, (b) the locations of 26 cities (red dots) and weather stations (blue triangles) in the YRD. The green rectangular regions represent the innermost domain and also the central YRD region. These cities in (b) include: the megacity Shanghai (SH); Hangzhou (HZ), Ningbo (NB), Jiaxing (JX), Huzhou (HZ1), Shaoxing (SX), Jinhua (JH), Zhoushan (ZS) and Taizhou (TZ) located in Zhejiang Province; Nanjing (NJ), Wuxi (WX), Changzhou (CZ), Suzhou (SZ), Nantong (NT), Yancheng (YC), Yangzhou (YZ), Zhenjiang (ZJ) and Taizhoushi (TZS) located in Jiangsu Province; and Hefei (HF), Wuhu (WH), Maanshan (MAS), Tongling (TL), Anqing (AQ), Chuzhou (CZ1), Chizhou (CZ2) and Xuancheng (XC) located in Anhui Province.

2 Materials and methods

2.1 Surface observations

Hourly O_3 concentrations monitored by the National Environmental Monitoring Center (NEMC) of China are used in this study. These data strictly follow the national monitoring standards HJ 654-2013 and HJ 193-2013 (http://www.cnemc.cn/jcgf/dqhj/), and can be available at https://quotsoft.net/air/, a mirror of data from the official NEMC real-time publishing platform (http://106.37.208.233:20035/). The nationwide observation network initially operated in 74 major cities sincein 2013, and it has grown to more than 1,500 stations covering 454 cities by 2017 (Lu et al., 2018). The urban hourly O_3 concentrations are average results of measurements at all monitoring sites for each city. The maximum daily 8-h running average (MDA8) O_3 concentrations are then calculated based on the hourly O_3 concentration with more than 18-h measurements in the day (Liao et al., 2017).

Meteorological data are provided by the National Climatic Data Center (NCDC), including 2-m air temperature (T_2), relative humidity (RH), 10-m –wind speed (WS_{10}) and direction (WD_{10}) , and relative humidityand cloud cover (CC), etc. These data as well as the technical documents recording the quality control, data collection and archive can be available at ftp://ftp.ncdc.noaa.gov/pub/data/noaa/isd-lite/. Locations of the surface observation stations are shown in Figure 1b. Specifically, the meteorological stations in the innermost domain include Pudong (Pd), Shanghai (Sh), Hongqiao (Hq) and Xiaoshan (Xs).

2.2 MODIS-based and USGS land use classifications

To investigate explore the effects impact of land-surface forcing land use on regional meteorology and O_3 evolution in the YRD, the two land use categories defaulted in WRF (MODIS-based and USGS land use classifications) are used to set up the first two sensitivity scenarios simulations (Table 2). The MODIS-based land cover product was created from 500-m MODIS Terra and Aqua satellite imagery (Friedl et al., 2010), and replaced USGS as the default settings in WRF since version 3.8. The USGS data primarily derived from the Advanced Very High Resolution Radiometer (AVHRR) from 1992 to 1993 at 1-km spatial resolution (Loveland et al., 2000), which is much earlier than the MODIS datareflects the distribution of cities in the late 1980s. Figure 2 presents the land cover maps in the innermost domain. The most obvious difference between MODIS and USGS comes from the urban fraction, which is related to the urban expansion caused byApparently, urban fraction with MODIS is much higher than USGS, indicating rapid urbanization in recent decades in the YRD. ~~The differences in urban land-surface forcing between USGS and MODIS mainly depend on urban expansion.~~ In addition~~Additionally~~, the Finer Resolution Observation and Monitoring-Global Land Cover in 2015 (GLC~~From-GLC_2015~~), which ~~can be considered as~~ is one of the latest (2015) and finest (30-m) land cover datasets (Gong et al., 2019), is quite consistent with the performance of MODIS in this region. This ~~further~~ confirms that urban fraction in~~with~~ MODIS is close to the reality. Thus, the MODIS data can generally refer to today's distribution of cities.

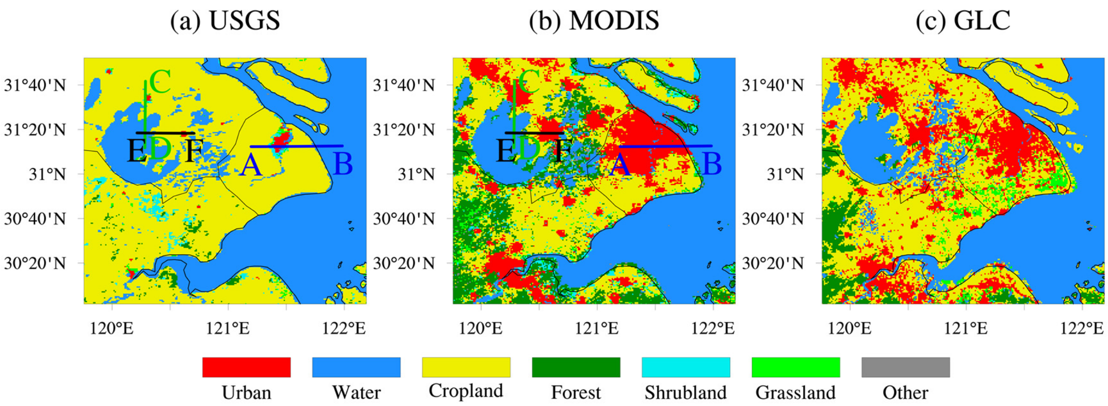

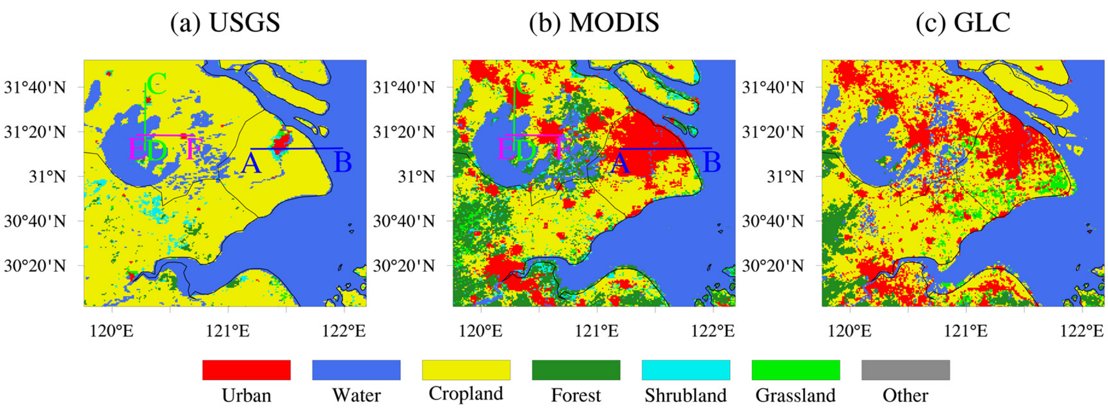

Figure 2. Land cover maps in the innermost domain, including the result of (a) USGS, (b) MODIS, and (c) GLC~~From-GLC_2015~~.

2.3 Anthropogenic heat flux modeling

Another scenario simulation incorporates~~involved~~ the urban canopy model with the gridded AH fluxes ~~is conducted to~~to diagnose the impact of~~estimate~~ AH ~~release in the central YRD~~. The AH fluxes were calculated based on the statistics data of energy consumption of China in 2016, and then were grided as 144 rows and 144 columns with a resolution at 2.5° using population density downloaded from Columbia University's Socioeconomic Data and Applications Center.are mainly the result of chemical energy or electrical energy that are converted to heat, thereby they can be quantified using the top-down energy inventory method. Based on the statistics data of energy consumption in 2016, the AH fluxes were calculated, and then were grided as 144 rows and 144 columns with a resolution at 2.5 arcmin using population density in China. AH fluxes with their diurnal variations are considered by adding them to the sensible heat flux from the urban canopy layer within the Single Layer Urban Canopy Model (SLUCM). The AH fluxes for each grid are determined by the fixed AH value for the urban land use category, the urban fraction value on each grid and the fixed temporal diurnal pattern. Details on the calculation as well as the distribution of AH fluxes, and how to add AH fluxes into the urban canopymodel can refer to Xie et al. (2016a, b). Figure 3 gives the spatial distribution of AH fluxes in the innermost domain. In the urban areas, the AH fluxes usually exceed 20 W m^{-2}. Some megabig cities, like Shanghai, can have a value of AH flux as high as 200 W m^{-2}. Except for the urban areas, the AH fluxes are generally less than 5 W m^{-2} in most parts of the YRD region. In particular, in those places where there is no human activity, the AH flux is 0.

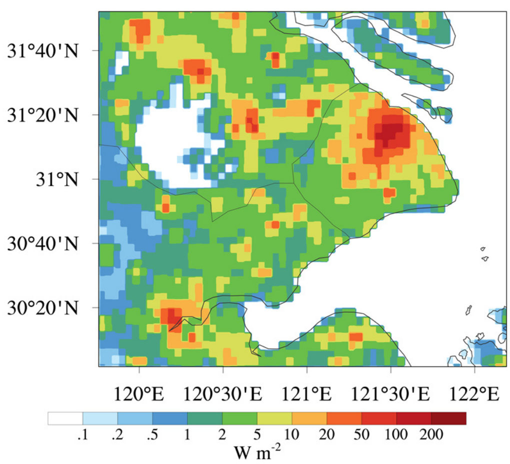

Figure 3. Spatial distribution of anthropogenic heat fluxes in the innermost domain.

2.4 Model set-up and experimental designs

In this study, the WRF-Chem version 3.9.1 is applied. The WRF-Chem model is a fully coupled online numerical weather prediction model with chemistry component (Grell et al., 2005), in which air qualitychemical and the meteorological component variables use the same coordinates, transport schemes and physics schemes in space and time. In this study, the WRF-Chem version 3.9.1 is applied. The initial and boundary conditions of meteorological fields are from the National Centers for Environmental Prediction (NCEP) global final analysis fields every 6 h with a spatial resolution of 1° × 1°. There are 32 vertical levels extending from the surface to 100 hPa with 12 levels located below 2 km to resolve the boundary layer processes. Furthermore, the domain and options for physical and chemical parameterization schemes are summarized in Table 1. The anthropogenic emissions are provided by the Multiresolution Emission Inventory for China (MEIC) in 2017 with a resolution of 0.25° (http://meicmodel.org/), which includes 10 air pollutants and CO_2 from power, industry, residential, transportation and agriculture sectors. The biogenic emissions are calculatedestimated online usingby the Model of Emissions of Gases and Aerosols from Nature (MEGAN) available in WRF-Chem (Guenther et al., 2006). As our main objective is to explore the response of O_3 to the meteorological changes induced by land use and AH, we use the same surface biogenic emission rates for different land use scenarios (Li et al., 2014, 2017). Further studies will be carried out to quantify the contribution of biogenic volatile organic compounds changed by meteorological conditions to O_3.

Table 1. The domains and major options for WRF-Chem

Items	Contents
Dimensions (x, y)	(101, 96), (146, 121), (236, 206)
Grid spacing (km)	25, 5, 1
Time step (s)	75
Microphysics	Purdue Lin microphysics scheme (Chen and Sun, 2002)
Longwave radiation	RRTM scheme (Mlawer et al., 1997)
Shortwave radiation	Goddard scheme (Kim and Wang, 2011)
Surface layer	Revised MM5 Monin-Obukhov scheme
Land-surface layer	Noah land-surface model (Chen and Dudhia, 2001)
Planetary boundary layer	YSU scheme (Hong et al., 2006)
Cumulus parameterization	Grell 3D ensemble scheme (Grell and Devenyi, 2002)

Gas-phase chemistry	RADM2 (Stockwelll et al., 1990)
Photolysis scheme	Fast-J photolysis (Fast et al., 2006)
Aerosol module	MADE/SORGAM (Schell et al., 2001)

As shown in Table 2, three numerical experiments are performed.~~ to study the effects of land-surface forcing and AH on meteorology and O_3 in the YRD.~~ The MODIS_noAH experiment is a control simulation with commonly used settings. Compared with MODIS_noAH, USGS_noAH selects the USGS land use classification~~data~~ at run-time through the geogrid program. Thus, the difference between the modeling results of MODIS_noAH and USGS_noAH can illustrate the changes caused by land use~~cover~~. As for the impact of AH, it can be identified by comparing the modeling results of MODIS_~~with~~AH and MODIS_noAH.~~ All three simulations run from 00:00 on 21 May to 00:00 on 4 June in 2017 with the first 88 h as spin-up time~~ To exclude the uncertainty conceivably caused by different configurations, all three simulations~~,~~ use~~sing~~ the same emission inventory, physical and chemical parameterization schemes (Table 1), running from 00:00 UTC 21 May to 00:00 UTC 4 June 2017 with the first 88 h as spin-up time.~~).~~

Table 2. The three numerical experiments.

Scenario~~Cases~~	Land use classification~~ategories~~	Whether to add AH
MODIS_noAH	MODIS-based	No
USGS_noAH	USGS	No
MODIS_~~with~~AH	MODIS-based	Yes

2.5 Model evaluation

To verify model performance, t~~T~~he simulation results in the innermost domain, including O_3 concentration, ~~2-m air temperature (~~T_2~~)~~, ~~relative humidity (~~RH~~)~~, ~~10-m wind speed (~~WS_{10} and ~~) and 10-m wind direction (~~WD_{10}~~)~~ are examined against the surface observations described in Sect. 2.1. The statistical metrics, including the mean bias (MB), root mean square error (RMSE) and correlation coefficient (COR), are also ~~used to evaluate the model performance~~calculated. They are defined as follows:

$$MB = \frac{1}{N}\sum_{i=1}^{N}(\mathrm{S}_i - \mathrm{O}_i), \tag{1}$$

$$RMSE = \sqrt{\frac{1}{N}\sum_{i=1}^{N}(\mathrm{S}_i - \mathrm{O}_i)^2}, \tag{2}$$

$$COR = \frac{\sum_{i=1}^{N}(\mathrm{S}_i - \bar{\mathrm{S}})(\mathrm{O}_i - \bar{\mathrm{O}})}{\sqrt{\sum_{i=1}^{N}(\mathrm{S}_i - \bar{\mathrm{S}})^2}\sqrt{\sum_{i=1}^{N}(\mathrm{O}_i - \bar{\mathrm{O}})^2}}, \tag{3}$$

where S_i and O_i are the simulations and observations, respectively. N is the total amount of valid data, and~~-~~ $\bar{\mathrm{S}}$ and~~-~~ $\bar{\mathrm{O}}$ represent the average of simulations and observations, respectively. Generally, the model performance is acceptable if the values of MB and $RMSE$ are close to 0, and that of COR is close to 1 (Xie et al., 2016a, b; Zhan et al., 2020).

3 Results and discussions

3.1 Regional O_3 pollution episodes in the YRD

~~Under adverse weather conditions~~On cloudless sunny days, regional O_3 pollution episodes occur frequently in the YRD (Gao et al., 2020; Zhan et al., 2021),~~.~~ which can ~~Sometimes, O_3 pollution can spread throughout the YRD and cause regional O_3 pollution,~~ affect~~ing~~ an area of up to 3.5 million square kilometers and harm~~ing~~ more than 200 million people. ~~Based on the surface O_3 observations, we define t~~The regional O_3 pollution ~~in the YRD~~ is generally defined as when more than half of the 26 typical cities in the YRD fail to meet the national O_3 standard (In China, the national ambient air quality standard for MDA8 O_3 is 160 μg m^{-3}). Based on the surface O_3 observations, ~~, and~~we ~~then~~ sort out all regional O_3 pollution episodes and the corresponding weather patterns from 2015 to 2019 (Table S1). There were 20, 19, 34, 28 and 30 regional O_3 pollution cases in the YRD from 2015 to 2019, respectively. These cases mainly occurred in April to October of each year, and were usually related to high pressure, uniform pressure field and typhoon activity.

Figure 4 further displays the monthly distribution of meteorological factors during the day (from 8:00 to 20:00 local time) when regional O_3 pollution occurs in the YRD. All the variables show significant monthly variations. The highest (lowest) temperature is found in July (April), and the relative humidity is highest in June. This may be related to the Meiyu in June, and the hot weather in July as the YRD is usually dominated by the western Pacific subtropical high after Meiyu. As for the cloud cover, the sky is covered with fewer clouds in October than other months. In addition, southeast wind prevails in the YRD from April to October under the influence of monsoon climate. The correlation coefficients between temperature, relative humidity, cloud cover, wind speed and MDA8 O_3 are 0.12, -0.34, -0.15 and 0.04, respectively. As shown in Figure 4, O_3 pollution episodes tendare likely to occur in the YRD on days characterized by high temperature, low relative humidity, cloudless sky and light wind (the weak correlation between wind speed and MDA8 O_3 is due to the small change in light wind).when the More specifically, on days when the temperature exceeds 20 ℃ (Figure 4b), the relative humidity is less than 80% (Figure 4c), the cloud cover is less than 5 okta (Figure 4d), and the wind speed is less than 3 m s^{-1} (Figure 4e) in the YRD. On the other handInterestingly, the local circulations induced by thermal differentiation areis clearest when in absence of clouds, radiative heating is strongest and wind is weakest. ThIn this case,us, both O_3 pollution and local circulations tend to appear in calm conditions characterized by high temperature, cloudless sky and weak wind, and the local circulation canwill inevitably have an impact on the distribution evolution of O_3 in this case.

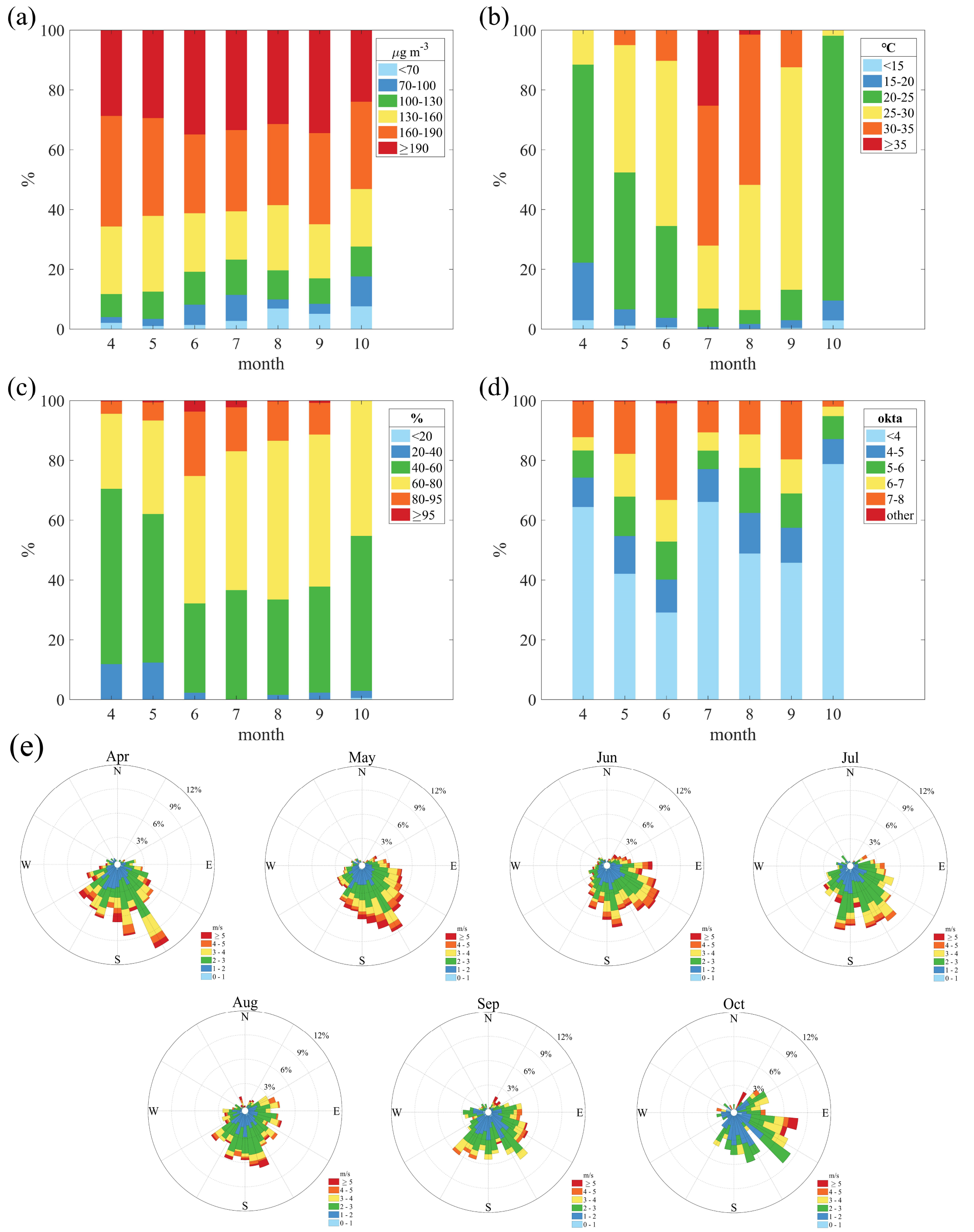

Figure 4. The monthly distribution of (a) MDA8 O_3, (b) temperature, (c) relative humidity, (d) cloud cover, and (e) wind speed and direction during the daytime (8:00 to 20:00 LT) when regional O_3 pollution occurs in the YRD.

3.2 Case selection

3.2.1 Case for O_3 pollution episode

For simplicity but without loss of generality, the longest-lasting regional O_3 pollution episodecase in Table S1 is selected to investigate the impacts of land-surface forcingland use –and AH on meteorology and O_3 pollution in the YRD. This 10-day regional O_3 pollution episode occurred from 25 May to 3 June in 2017 (Table S1). Dominated by high pressure/uniform pressure field (Figure S1), high O_3 concentrations are accompanied by high air temperature, low relative humidity, light wind and shallow cloud cover dDuring this smog episodeperiod., Anan average of 18 out of the 26 cities experienced O_3 pollution every day with, and the MDA8 O_3 concentrations ranged ranged from 80.0168.1 to 26905.01 μg m^{-3} in the YRD. Moreover, the daily maximum air temperature ranged from 28.5 to 33.9 °C over the central YRD (the innermost domain) under high pressure/uniform pressure field (Figure S1)With regard to the meteorological factors, T_2 ranged from 12.9 to 33.5 °C, with an average of 26.4 °C; RH ranged from 26.6 to 99.4 %, with an average of 58.6 %; WS_{10} ranged from 0.5 to 10.8 m s^{-1}, with an average of 2.8 m s^{-1}; CC ranged from 0 to 8.4 okta, with an average of 4.2 okta (Table 3). The values of these meteorological factors meet the standards in previous section, and can cover both the whole YRD and the central YRD region (the innermost domain). Therefore, , tThis O_3 pollution episode not onlycase meets the requirements of calm weather and high O_3 concentration but also clam weather conditions. And the relatively long duration– provides relatively universal also provide a representative results.

Table 3. Mean, minimum and maximum of MDA8 O_3, T_2, RH, WS_{10} and CC during the daytime from 25 May to 3 June 2017.

	The YRD region			The central YRD region		
	Mean	Minimum	Maximum	Mean	Minimum	Maximum
MDA8 O_3 (μg m^{-3})	182.1	80.0	269.0	177.8	118.0	251.0
T_2 (°C)	26.4	12.9	33.5	26.7	21.4	29.8
RH (%)	58.6	26.6	99.4	52.9	33.8	73.7
WS_{10} (m s^{-1})	2.8	0.5	10.8	3.6	1.6	6.0
CC (okta)	4.2	0	8.4	3.3	0	7.4

3.2.2 Evaluation of model performance

To evaluate the model performanceIn this study, three numerical experiments are conducted using WRF-Chem (Sect. 2.4) during the period of the previously mentioned O_3 episode. Tthe simulation results in the innermost domain are validated in the innermost domain by comparing with the observational data. Table ~~5~~ 4 presents the statistical metrics in meteorological factors~~variables that includes 2-m air temperature (T_2), relative humidity (RH), 10-m wind speed (WS_{10}) and direction (WD_{10})~~. Figure 5 further illustrates the time series of~~comparisons between~~ these meteorological factors and their modeling results. T_2 is reasonably well simulated as the ~~mean~~ CORs (the mean of all the sites) are 0.87~~5~~, 0.86~~5~~ and 0.86~~3~~ in MODIS_noAH, USGS_noAH and MODIS_AH, respectively. The small negative MBs at all sites suggest that our simulations underestimate T_2 to some extent, though this light underestimation is acceptable because of the small ~~mean~~ RMSEs (2.3, 3.1 and 2.3 °C). The ~~mean~~ MBs for T_2 in USGS_noAH, MODIS_noAH and MODIS_AH are -2.4, -1.0, and -0.8 °C, indicting an improvement in temperature when new land use and AH are taken into account. Th~~ese results~~is can also be confirmed by Figure 5a. With respect to RH, the ~~mean~~ CORs are 0.82~~3~~, 0.75~~3~~ and 0.83~~25~~ for ~~the three numerical experiments~~MODIS_noAH, USGS_noAH and MODIS_AH, respectively. Thus, a~~A~~ll three simulations can well capture the diurnal variation of RH, but have different performance on different sites (Figure 5b). In USGS_noAH, RH is overestimated at all sites, especially Pudong site with~~, and~~ the ~~mean~~ MB is 11.2%. While RH is ~~only~~ overestimated at the two coastal sites (Pudong and Shanghai) but underestimated at other two sites (Hongqiao and Xiaoshan) in MODIS_noAH and MODIS_AH. Moreover, USGS_noAH has the highest ~~mean~~ RMSEs of RH (16.3%), followed by MODIS_AH (12.4%) and MODIS_noAH (12.1%). As for WS_{10}, the modeling values are slightly overestimated at all sites in all three simulations. The overestimation of WS_{10} may partly be attributed to the unresolved terrain features by the default surface drag parameterization causing an overestimation of wind speed ~~in particular~~especially at low values (Jimenez and Dudhia, 2012). In particular~~Specially~~, WS_{10} in USGS_noAH is the most overestimated, followed by MODIS_AH and MODIS_noAH ~~,~~with the ~~mean~~ MBs are 1.2, 1.0 and 0.8 m s^{-1}, respectively. ~~Additionally~~In addition, ~~a~~ high ~~mean~~ MBs of WS_{10} are~~is found to~~ corresponding to ~~a~~ high ~~mean~~ RMSEs (1.9, 1.8 and 1.7 m s^{-1}) in our simulations. In terms of WD_{10}, the model captures well the shift in wind direction during the study period (Figure 5d). Thus, our modeling results of wind speed and direction basically reflect the characteristics of wind fields. In summary, both the statistical metrics in Table ~~3~~ 4 and time series in Figure 5 ~~illustrate~~ indicate that all three~~e~~ numerical experiments can capture ~~reflect~~ the major changes~~characteristics~~ about~~of~~ meteorological ~~conditions~~ factors during this O_3 pollution episode. Nevertheless, updating the~~sing~~ ~~new~~ land-use ~~data~~ and adding AH can somewhat reduce the underestimation of T_2 and the overestimation of RH and WS_{10} in models to some extent.

Table 34. Statistical metrics in meteorological variables between observations and simulations.

Variables	Site		MODIS_noAH				USGS_noAH				MODIS_AH			
		$\bar{O}$[a]	$\bar{S}$[b]	MB[c]	RMSE[d]	COR[e]	$\bar{S}$	MB	RMSE	COR	$\bar{S}$	MB	RMSE	COR
T_2	Pd	23.2	21.5	-1.7	2.4	0.89	20.7	-2.5	3.8	0.70	21.5	-1.7	2.4	0.89
(℃)	Sh	24.6	23.9	-0.7	2.2	0.87	22.5	-2.1	2.7	0.90	24.2	-0.5	2.3	0.84
	Hq	25.3	24.4	-0.9	2.0	0.89	22.7	-2.6	3.0	0.95	24.8	-0.5	1.9	0.89
	Xs	25.9	25.1	-0.8	2.4	0.85	23.8	-2.2	2.8	0.91	25.5	-0.4	2.4	0.83
RH	Pd	69.1	77.7	8.6	13.5	0.81	86.2	17.2	23.4	0.45	77.7	8.7	13.3	0.83
(%)	Sh	59.3	60.6	1.3	11.7	0.81	71.1	11.8	16.1	0.81	59.4	0.1	12.4	0.78
	Hq	59.5	57.7	-1.8	9.8	0.88	70.6	11.1	14.5	0.89	56.2	-3.3	9.8	0.89
	Xs	60.6	55.4	-5.2	13.5	0.79	65.3	4.8	11.3	0.86	53.5	-7.1	14.1	0.80
WS_{10}	Pd	4.1	4.1	0.0	1.4	0.47	5.5	1.3	2.1	0.35	4.2	0.1	1.3	0.51
(m s^{-1})	Sh	2.5	4.2	1.7	2.2	0.36	4.5	2.0	2.4	0.54	4.3	1.9	2.3	0.35
	Hq	3.7	3.9	0.2	1.2	0.54	3.9	0.2	1.2	0.53	4.2	0.5	1.3	0.50
	Xs	2.3	3.6	1.3	2.0	0.26	3.4	1.1	1.8	0.30	3.8	1.5	2.1	0.24
WD_{10}	Pd	160.4	136.1	-26.2	78.7	0.42	148.1	-14.3	55.1	0.72	137.3	-24.7	77.5	0.42
(°)	Sh	141.6	146.4	4.8	66.4	0.60	141.7	0.1	63.9	0.59	142.6	1.0	69.9	0.56
	Hq	159.7	140.2	-23.4	80.2	0.46	153.1	-10.6	74.9	0.52	142.8	-20.4	91.8	0.29
	Xs	188.6	160.2	-28.4	99.5	0.48	161.4	-27.3	109.6	0.35	152.0	-36.6	109.9	0.38

[a] $\bar{O}$ and [b] $\bar{S}$ indicate the average of observations and simulations, respectively. [c] MB indicates the mean bias, [d] RMSE indicates the root mean square error and [e] COR indicate the correlation coefficient, with statistically significant at 99% confident level.

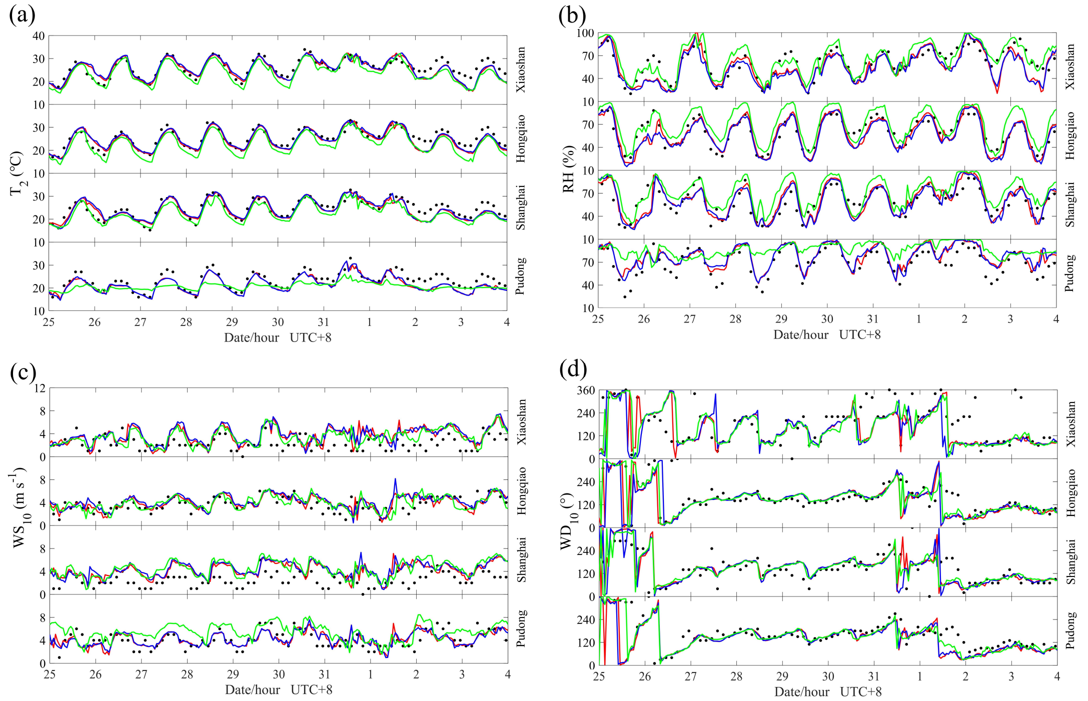

Figure 5. Time series of T_2, RH, WS_{10} and WD_{10} for observations and simulations at different weather~~meteorological~~ stations. The black dots are the surface observations. The simulation results of MODIS_noAH, USGS_noAH and MODIS_~~with~~AH are shown in red, green and blue lines, respectively.

Table ~~4~~ 5 lists the statistical metrics in O_3, and Figure 6 gives the hourly variations of O_3 for observations and simulations in~~at~~ different citie~~site~~s. With high CORs (the~~ mean~~ CORs are 0.80, 0.81 and 0.80 in MODIS_noAH, USGS_noAH and MODIS_AH, respectively), all three simulations~~ can~~ well reproduce the diurnal variation of O_3, which ~~shows~~is that O_3 concentration reaches its maximum in the afternoon and gradually decreases to its minimum in the morning. The magnitudes of O_3 modeling results ~~is~~ are reasonable (Figure 6), but the peak and valley values of O_3 simulations are sometimes differ ~~greatly~~ from the observations, especially the peak value, like~~like~~ Huzhou. ~~This may be related to the resolution of the emission inventory and the distribution of O_3 precursors.~~ Considering the relatively low ~~mean~~ MBs (6.9, -1.6 and 9.0 μg m^{-3}) and~~ mean~~ RMSEs (49.3, 46.2 and 49.0 μg m^{-3}), the modeling results of O_3 are generally reasonable and acceptable.

Table 45. Statistical metrics in O_3 (μg m^{-3}) between observations and simulations.

Case	Index	CitySite						
		CZ	WX	SZ	SH	HZ1	JX	HZ
	$\bar{O}$	89.7	141.8	121.7	112.8	95.8	113.2	104.8
MODIS_noAH	$\bar{S}$	123.2	117.6	116.2	103.4	128.1	112.5	127.5
	MB	33.3	-24.2	-5.6	-9.1	32.1	-0.6	22.7
	RMSE	53.8	49.1	42.8	36.4	59.9	44.4	58.6
	COR	0.85	0.83	0.82	0.80	0.83	0.78	0.71
USGS_noAH	$\bar{S}$	108.1	106.8	107.1	93.8	118.6	111.0	122.5
	MB	18.5	-35.0	-14.7	-18.9	23.0	-2.0	18.0
	RMSE	43.5	56.0	44.7	37.7	50.1	41.1	50.0
	COR	0.83	0.81	0.80	0.81	0.82	0.80	0.77
MODIS_AH	$\bar{S}$	124.5	119.8	119.1	108.0	130.3	113.7	127.8
	MB	34.7	-21.9	-2.7	-4.6	34.3	0.6	23.0
	RMSE	53.5	47.3	42.4	37.4	59.4	44.7	58.2
	COR	0.84	0.83	0.81	0.80	0.82	0.78	0.71

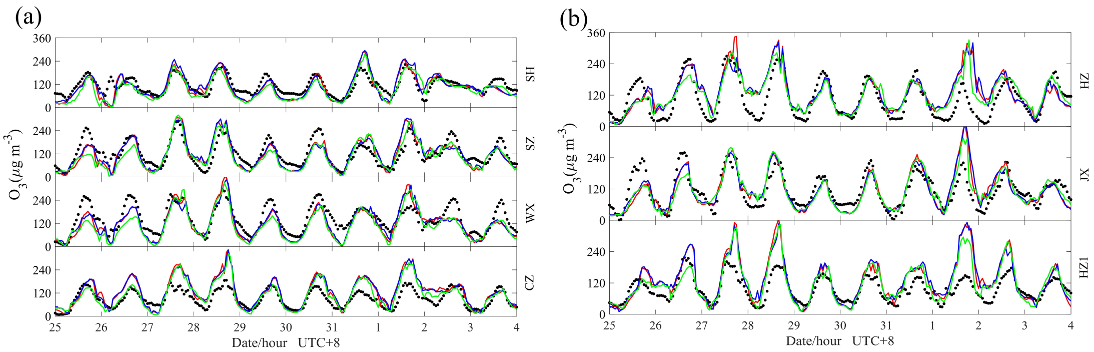

Figure 6. Same as Figure 5, but for O_3.

Above all, the WRF-Chem model using our configuration has a good capability in simulating the meteorological factorsy and O_3 air quality over the studied region in this study. In addition, iIt is still noteworthy that the object of inter-comparisons between the three numerical experiments is are not to determine which setting is the most skillful in reproducing the observations. Rather, it is to diagnose and understand the changedifferences induced by land-surface forcingland use and AH, and then to provide valuable insight into the formation of the O_3 pollution episodes response of O_3 to these changes.

3.3 Overall behaviors of O_3 and local circulations

Based on the results of the control simulation (MODIS_noAH), we first give an overall behavior of O_3 and local circulations during the study period. T And then the changesdifferences induced by land useland-surface forcing and AH are discussed via inter-comparisons between differentthe numerical experimentsscenarios simulations. Thereby, only difference plots between USGS_noAH/MODIS_withAH and MODIS_noAH are shown in this paper, andbut the corresponding original plots for USGS_noAH and /MODIS_withAH can be found in the supplementary materials (Figure S2-57).

3.3.1 Spatiotemporal variations of O_3

As show in Figure 7, O_3 concentration began to rise around 8:00 local time (LT = UTC + 8 h) after sunrise, and became noticeable after only 3 hours (Figure 7a and h). During this stage, the nocturnal residual layer vanished due to the development of the convective boundary layer (Figure 8). The O_3-rich air mass in the residual layer was mixed with the O_3-poor air mass on the ground, which enhanced the surface O_3 in the morning (Hu et al., 2018). Around 11:00 LT, the convective boundary layer was established (Figure 8), and high O_3 produced by photochemical reactions appeared over the central YRD and persisted until 18:00 LT (Figure 7b and , 7c and 8). The maximum O_3 production was in the middle of the boundary layer (~800 m) instead of at the surface (Figure 8). After sunset, surface O_3 concentrations generally decreased sharply due to nitrogen oxide (NO) titration, and reached its minimum in the early morning. The loss of O_3 caused by NO titration almost ceased around 2:00 LT when O_3 was at its lowest level of the day (Figure 7f and g). In general, O_3 has a typical diurnal variation with high concentration in the daytime and low concentration at night. This is consistent with the observationsresults in Figure 6, and this rule of O_3 can be applied to most parts of the world. Therefore, the situation during the daytime (wWe select 11:00, 14:00, 17:00 and 20:00 LT in this study) should be paid attention to when it comes to O_3 pollution.

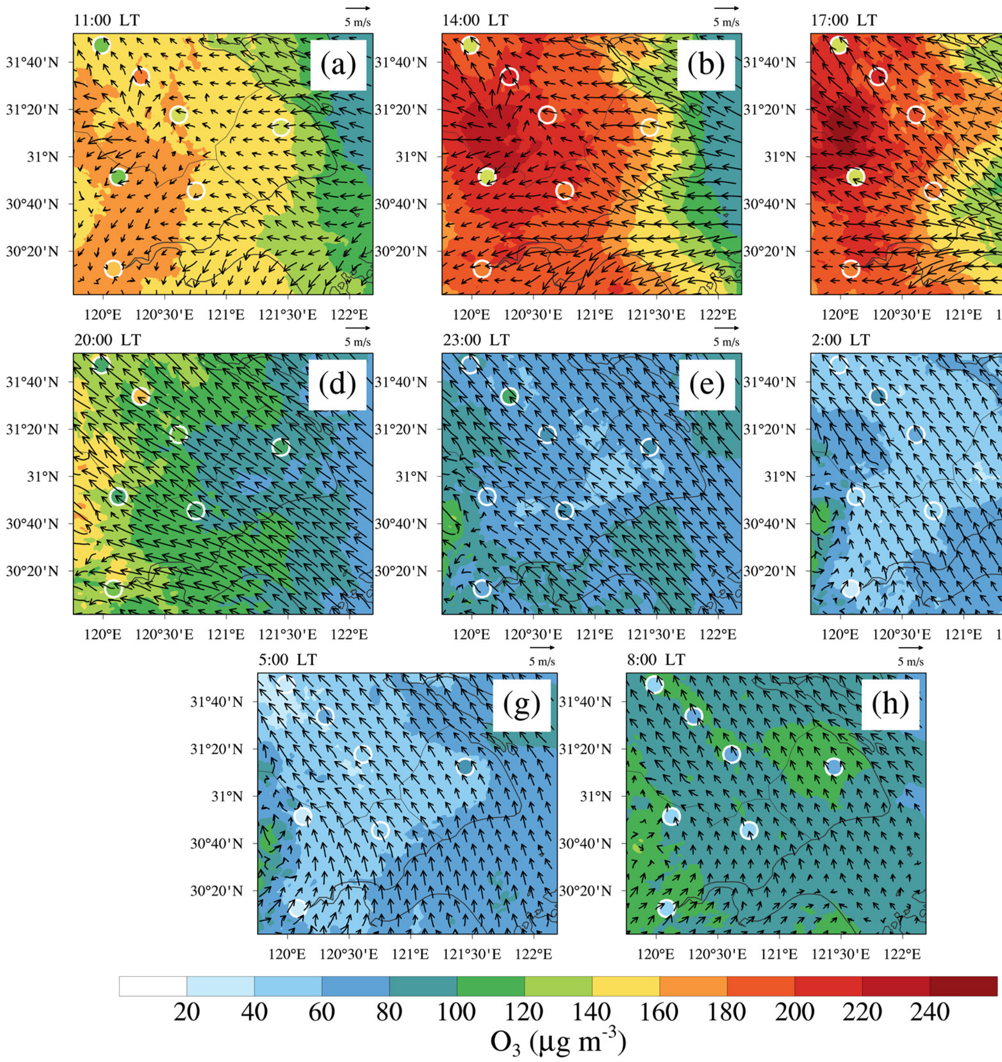
11:00 LT
(a)
14:00 LT
(b)
17:00 LT
(c)
20:00 LT
(d)
23:00 LT
(e)
2:00 LT
(f)
5:00 LT
(g)
8:00 LT
(h)
5 m/s
31°40'N
31°20'N
31°N
30°40'N
30°20'N
120°E
120°30'E
121°E
121°30'E
122°E
20 40 60 80 100 120 140 160 180 200 220 240
O_3 (μg m^{-3})

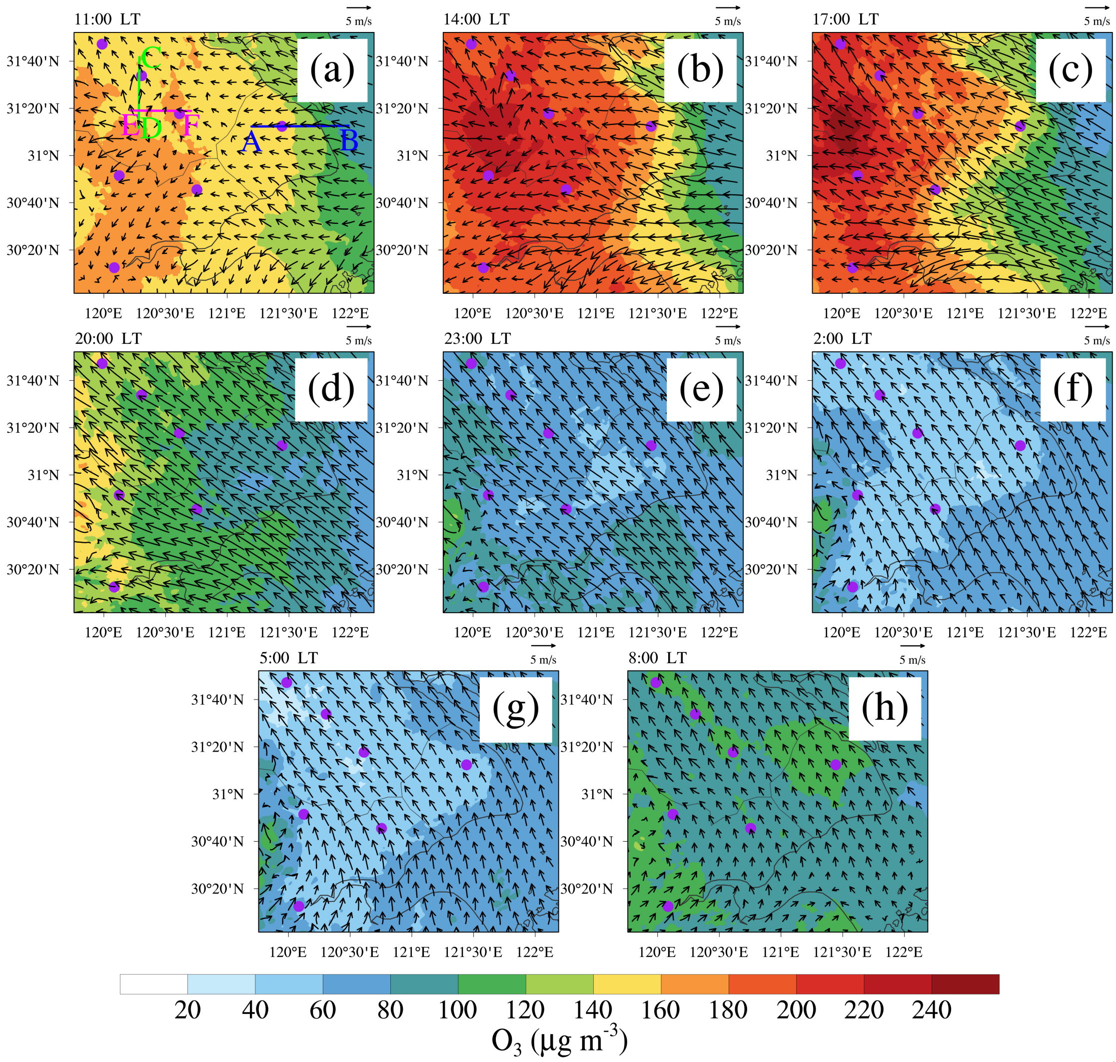

Figure 7. Horizontal distributions of O_3 and wind at the lowest model level in MODIS_noAH. (a), (b), (c) and (d) are the results at 11:00, 14:00, 17:00 and 20:00 LT, referring to the daytime. (e), (f), (g) and (h) are the results at 23:00, 2:00, 5:00 and 8:00 LT, referring to the night. The observations in different cities are overlaid using colored circles ~~purple dots represent the locations of cities (red dots in Figure 1b) in the innermost domain~~. To obtain ~~general~~ universal feature, all results are the average of the study period, and the same for the subsequent results.

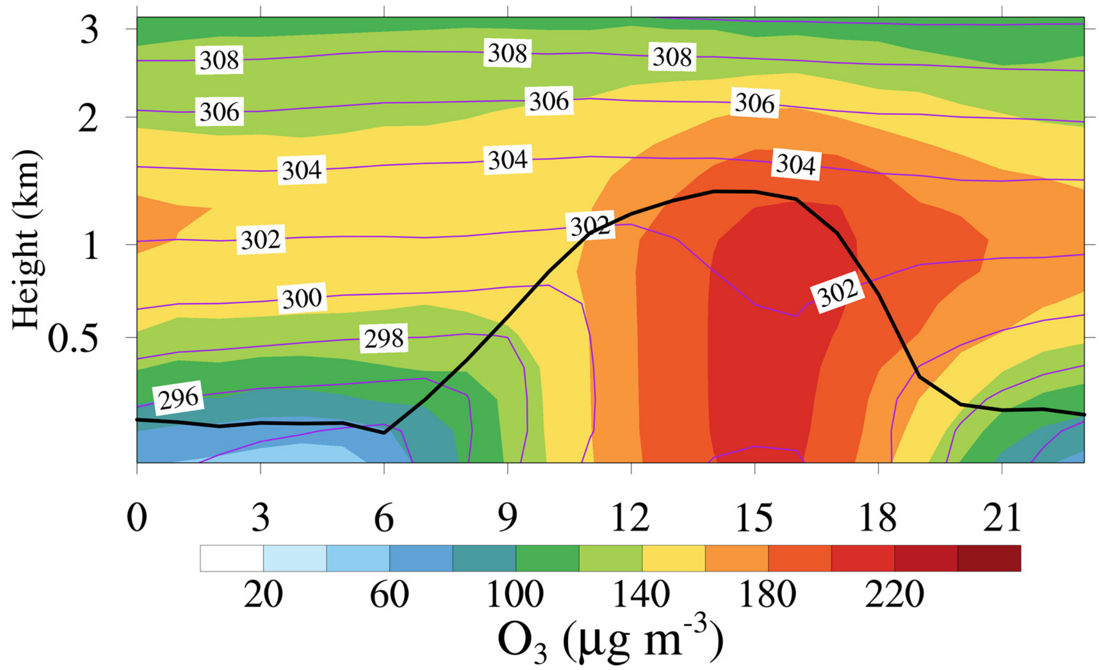

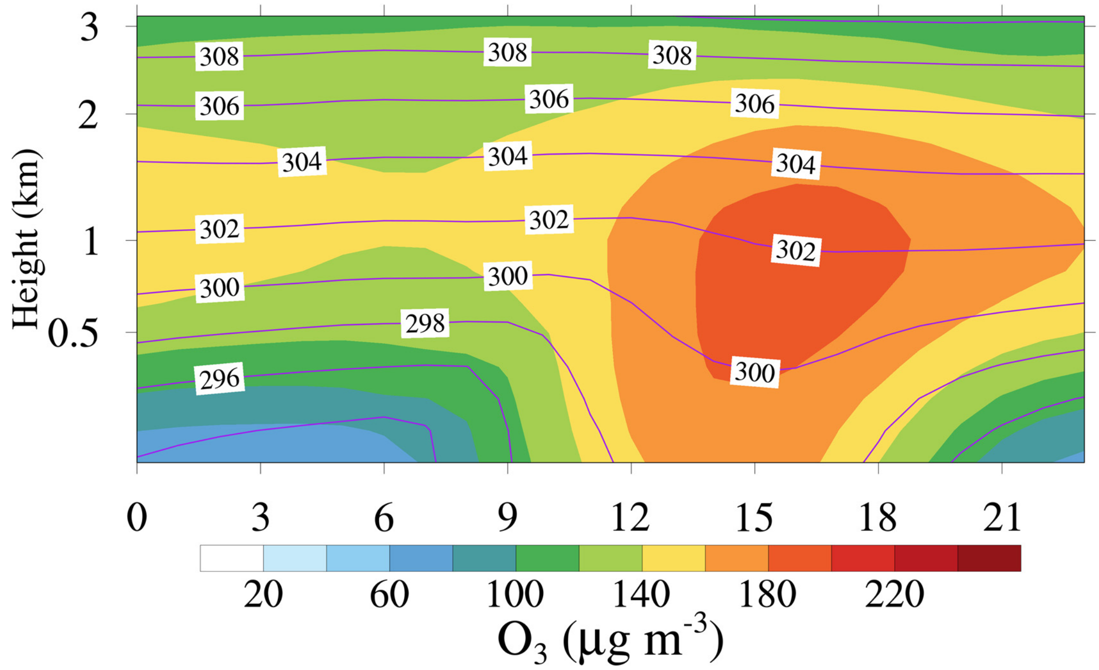

Figure 8. Temporal-vertical distribution of O_3 and potential temperature ~~over the innermost domain~~covering the CZ, WX, SZ, SH, HZ1, JX and HZ over the innermost domain of ~~in~~ MODIS_noAH.

3.3.2 Sea and lake breezes

As shown in Figure 7a and b, high O_3 concentration in the central YRD tended to appear in the converging airflows associated with the sea breeze, the lake breeze and background southeast wind (Figure 4e).in the areas where the local circulations meet the background dominant winds (the southeast wind), the converging airflows make O_3 concentrations higher than those in the surrounding areas. Furthermore, Tthe typical local circulations in the central YRD are the sea and the lake breezes around the Tai Lake. In this study, tthe sea -breeze and the background southeast wind were usually in the same direction, and thereby sea breeze –affectededed a wide area and lasted a long time., which may be related to the local background field since they are mostly in same direction, and it is difficult to separate the sea-breeze from the southeast wind. The sea -breeze was obvious around 14:00 LT and matured around 17:00 LT, and continuously transported high O_3 from coastal to the inland areas during this period (Figure 7b-d). Compared with the sea -breeze, the lake -breeze had a much smaller influencing area and a shorter duration. Around 11:00 LT, the lake -breeze was established. It reached its maximum intensity around 14:00 LT, and then disappeared sharply due to the predominant southeast windsea-breeze (Figure 7b and c). Both the sea and the lake breezes are the typical local circulations in the YRD, which playsplayed important roles in the horizontal distributions of O_3 over this region in the central YRD.

SinceAs the coastline is generally north-south (Figure 1b), the cross sections along blue line AB depicted in Figure 2a7a are illustrated to show representative example of the vertical structure of the sea breezes (Figure 9a-c). By 11:00 LT, tThe sea -breeze below 500m had already developeddd by 11:00 LT. A The sea -breeze front was found in front of Shanghai (~121.6°E), with a height of 1.5 km. Around 14:00 LT, tThe speed of sea -breeze increased around 14:00 LT, which can exceeded 5 m s^{-1}. The intensified sea -breeze front movedpenetrated inland for a distance of 20-30 km, and the sea-breeze front (~121.4°E), and lifted the boundary layer top over Shanghai upwas elevated to ~2 km (Figure 9b). Around 17:00 LT, sStrong sea -breeze swept across the central YRD around 17:00 LT, reducing the O_3 concentration near the surface in Shanghaicoastal areas. But the O_3 in the mixed layer still maintained a high level, which maycan result in an O_3-rich reservoir forming in the nocturnal residual layer (Figure 9ce and 8). The penetration of sea -breeze front and its effect on surface O_3 arecan be also observed in other coastal regions, such as the Pearl River Delta Region (You et al., 2019), Taiwan (Lin et al., 2007), the Athens basin (Mavrakou et al., 2012) and Paulo (Freitas et al., 2007).

As for the lake breezes, the cross sections along green line CD (Figure 9d-f) and black line EF in Figure 2a(Figure 9g-i) are given since the lake is usually inside the land so that the lake breezess can have different directions. The lake -breeze was established when the surface wind was weak by 11:00 LT (Figure 9d and g) though it was shallow at that time. Around 14:00 LT, the lake -breeze strengthened. The extension of the lake -breeze circulation zone can even reach up to 2 km in the vertical dimension (Figure 9e). The offshore flow (~ 2 m s^{-1}) of the lake -breeze circulation (~2 m s^{-1}) transported high O_3 concentration from the urban areas to the lake, while the onshore flow blew the O_3 back to urban areas (Figure 9e and h). Thus, the net effect ofis that the lake -breeze is to "accelerated" the vertical mixing of O_3 in the boundary layer, resulting in high concentration of surface O_3 in the lakeside cities. The high surface O_3 concentration caused by the lake breezes This was also reported inhas also been confirmed near other lakeside citiess, such as the Lake Michigan (Lennartson and Schwartz, 2002), the Great Lakes (Sills et al., 2011) and the Great Salt Lake (Blaylock et al., 2017). By 17:00 LTFinally, the lake -breeze was destroyed by the prevailing southwest wind by 17:00 LT. disappeared.

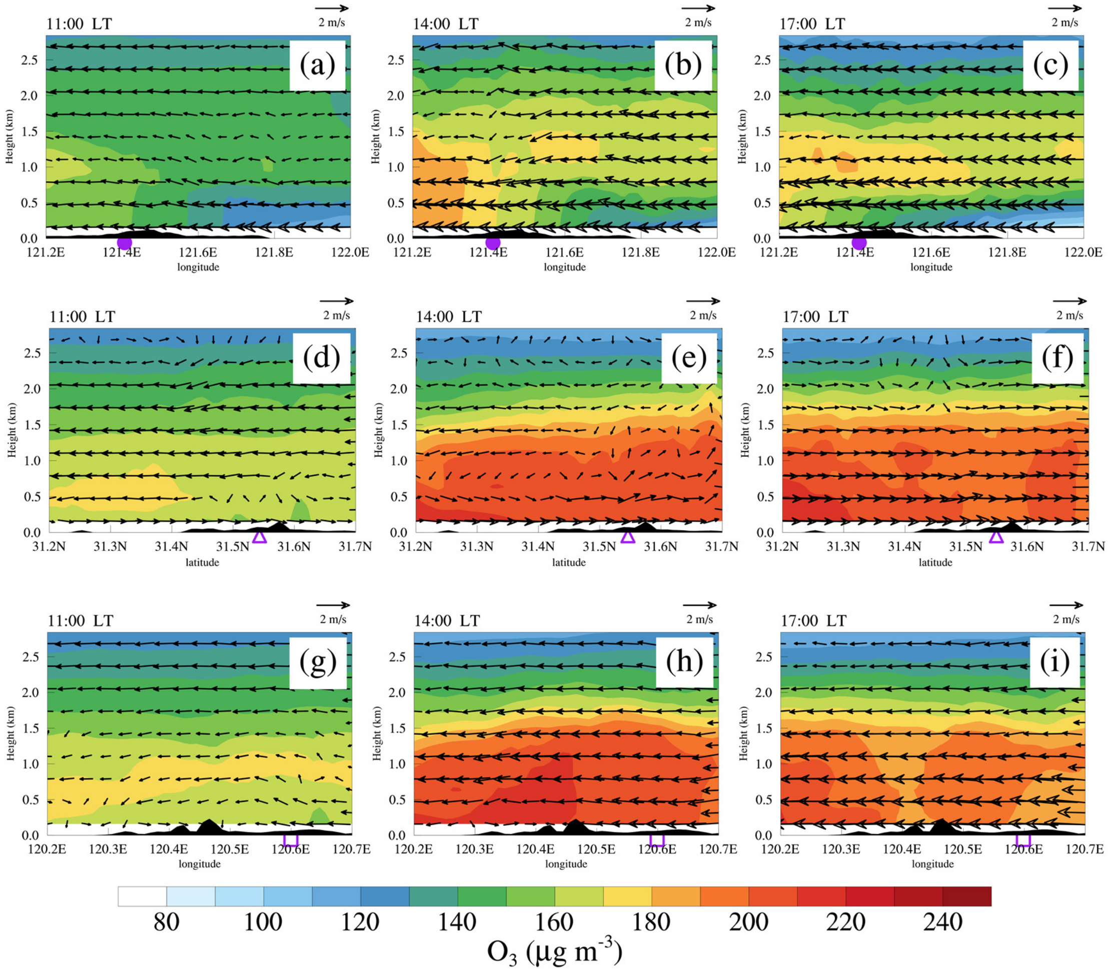

11:00 LT
14:00 LT
17:00 LT
2 m/s
(a)
(b)
(c)
(d)
(e)
(f)
(g)
(h)
(i)
Height (km)
0.0
0.5
1.0
1.5
2.0
2.5
121.2E
121.4E
121.6E
121.8E
122.0E
longitude
31.2N
31.3N
31.4N
31.5N
31.6N
31.7N
latitude
120.2E
120.3E
120.4E
120.5E
120.6E
120.7E
80
100
120
140
160
180
200
220
240
O3 (μg m-3)

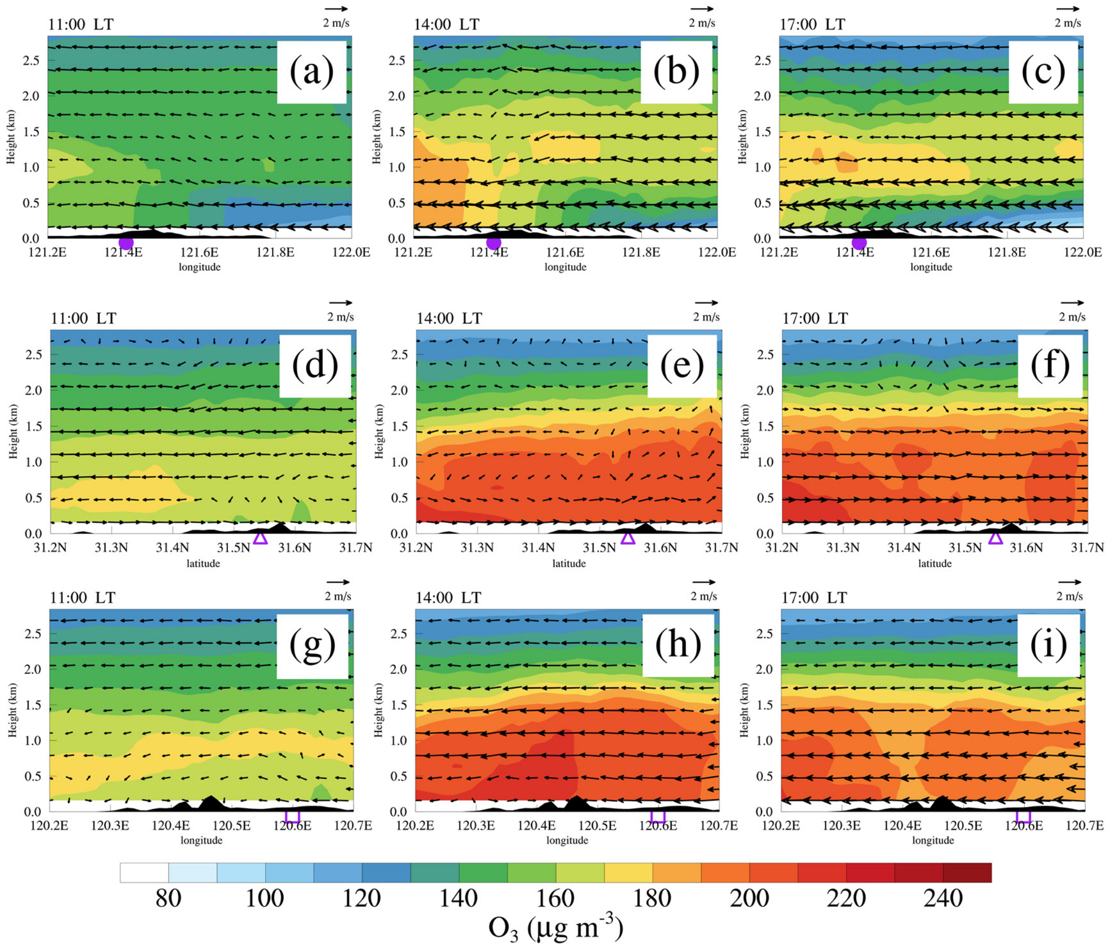

Figure 9. Vertical cross sections of O_3 and wind for the sea ~~-~~breeze at (a) 11:00, (b) 14:00 and (c) 17:00 LT along blue~~the~~ line AB in Figure 2~~7~~a. (d), (e) and (f) are the same as (a), (b) and (c), respectively, but for the lake ~~-~~breeze along green~~the~~ line CD in Figure 2~~7~~a. (g), (h) and (i) are also the same as (a), (b) and (c), respectively, but for the lake ~~-~~breeze along black~~the~~ line EF in Figure 2~~7~~a. The purple dots, triangles and rectangles represent the locations of Shanghai, Wuxi and Suzhou, respectively. The black shaded areas represent the terrain, and the terrain has been multiplied by a factor of 10 when plotting.

3.4 Impacts of ~~land-surface forcing~~ land use on meteorology and O_3

3.4.1 The changes in horizontal direction

Figure 10 presents the spatial differences of the main factors (~~, including O_3,~~ T_2, PBLH, ~~and~~ WS_{10} and O_3)~~,~~ between MODIS_noAH and USGS_noAH. Land use changes via urban expansion can enhance surface heating through upward sensible heat fluxes so that T_2 will increase. As shown in Figure 10a-d, the spatial pattern of remarkable warming effect for T_2 was consistent with the urban-fraction change associated with the urbanization (Figure 2a and b), which is the positive temperature anomaly mainly appeared in cities and their surrounding areas. In megacities like Shanghai, T_2 increased by even 3 °C. The change in PBLH was similar to that in T_2 because the warming up of T_2 was conductive to the vertical movement in the boundary layer, which increased the PBLH (Figure 10e-h). The maximum positive change of PBLH can reach up to 500 m at noon but down to 100 m after sunset. With regard to the WS_{10}, it decreased in the MODIS_noAH (Figure 10i-l), with a maximum decrease up to 1.5 m s^{-1} in Hangzhou around 17:00 LT. This is because the roughness of cities and forest is larger than that of cropland (Figure 2a and b). Apart from the abovementioned meteorological factors, urban expansion also increased the surface O_3 concentration (Figure 10m-p). The largest increment of O_3 appeared in the afternoon, with a value of 20 μg m^{-3} around 17:00 LT in Changzhou. In addition to these results, it is noteworthy that there were confusing "false" changes at the junction of land and sea/lake, especially for meteorological factors, such as T_2 and WS_{10}. This was caused by the different treatment of the MODIS-based and USGS land use classifications at the boundary conditions of land versus water instead of urban expansion. Obviously, higher O_3 was produced in the MODIS_noAH, indicating that urban expansion will increase surface O_3 concentrations. The largest increment of O_3 occurred in the afternoon, with a value of 20 μg m^{-3} around 17:00 LT in Changzhou. T_2 is directly affected by the land-atmosphere heat fluxes resulting from land-surface forcing. The spatial pattern of remarkable warming effect for T_2 was consistent with the urban-fraction change (Figure 2a and b), which is that the positive temperature anomaly often appeared in large cities and their surrounding areas. This positive forcing for T_2 is associated with the enhanced surface heating through upward sensible heat fluxes during the day. In megacities like Shanghai, T_2 can increase by 3 °C. It should be noted that there was a confusing "false" warming at the junction of land and sea/lake, which was mainly caused by the different treatment of the MODIS-based and USGS land use classifications at the boundary conditions of land versus water (Figure 2a and b). The change in PBLH was similar to that in T_2, but it was less obvious after sunset around 20:00 LT. This is because that the warming up of T_2 can enhance the vertical air movement in the boundary layer and thereby increase the PBLH. The maximum positive change of PBLH reached up to 500 m in the urban areas at noon but downed to 100 m after sunset. The roughness of cities and forest is greater than that of cropland, so there was a decrease in WS_{10} in the MODIS_noAH (Figure 9m-p), with a maximum decrease up to 1.5 m s^{-1}

~~in Hangzhou around 17:00 LT.~~

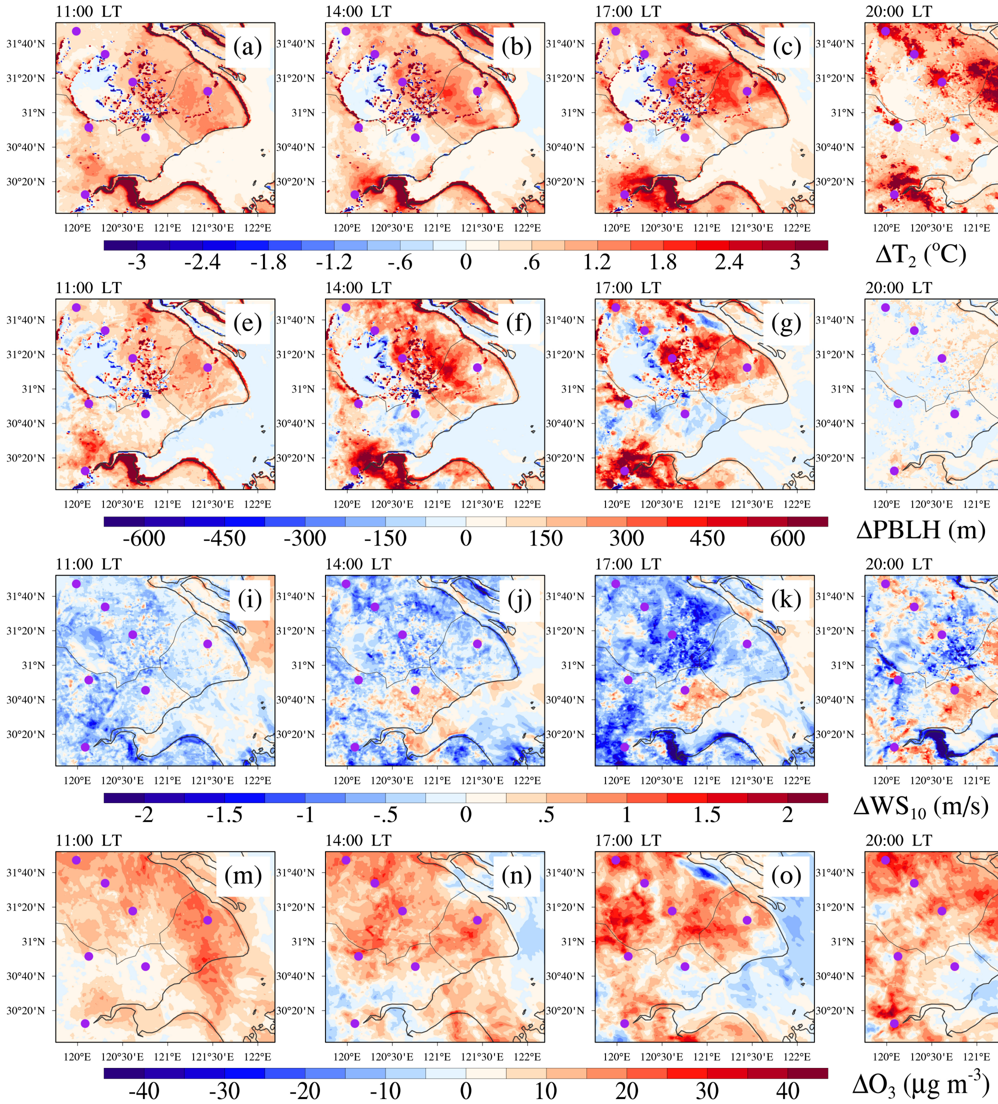

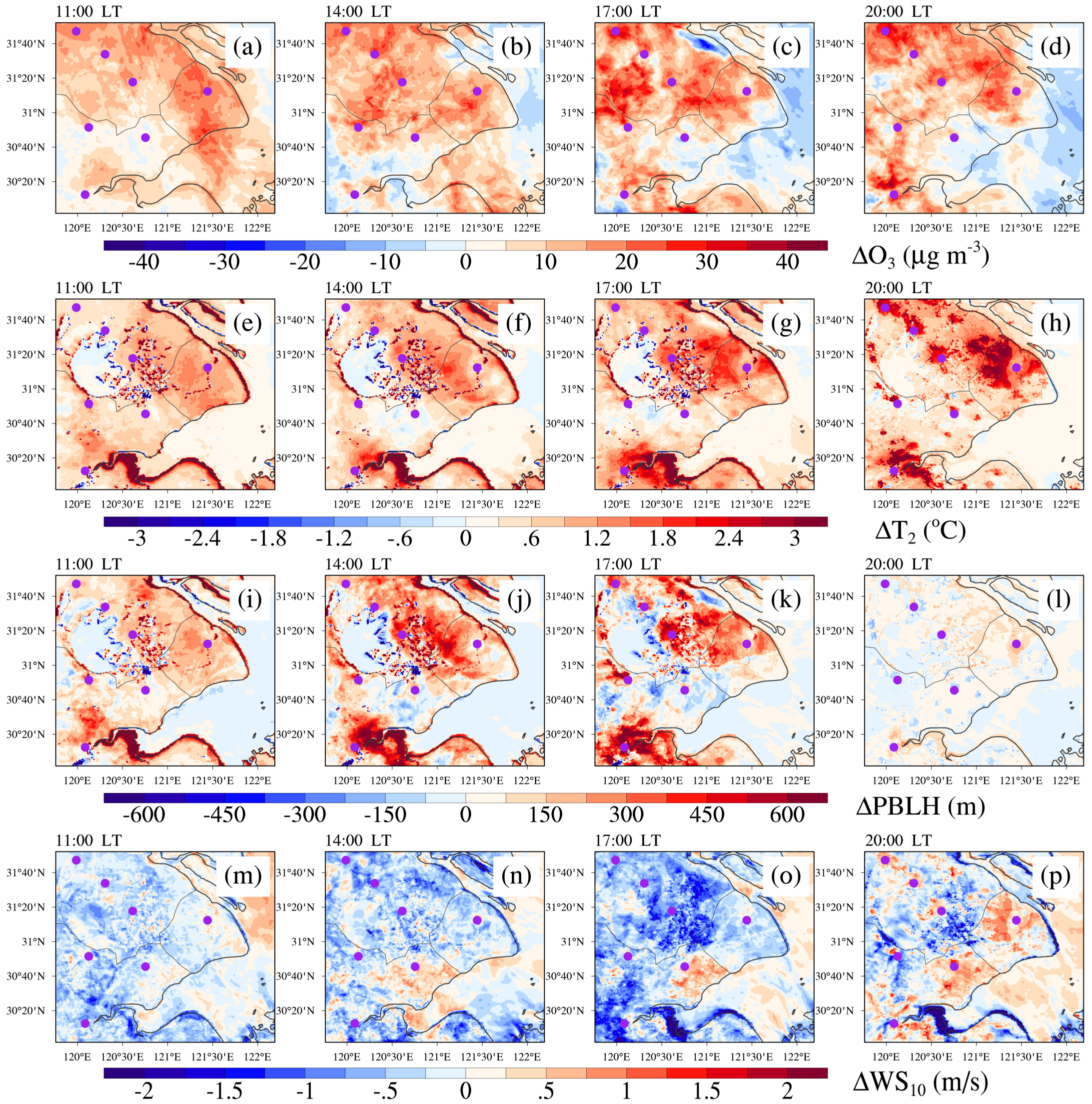

Figure 10. Horizontal distributions of the differences ofthe (a-d) T_2 O_3, (e-h) PBLH T_2, (i-l) WS_{10}PBLH and (m-p) O_3 WS_{10} differences between MODIS_noAH and USGS_noAH (MODIS_noAH – USGS_noAH) duringat different times (11:00, 14:00, 17:00 and 20:00 LT) of the daytime. The purple dots represent the locations of cities (red dots in Figure 1b) in the innermost domain.

3.4.2 The changes in vertical direction

Urban expansion not only alters the meteorological factors, but also the local circulations. As shown in Figure 11a-c, the sea -breeze below 500 m increased by ~1-2 m s^{-1} due to the existence of the cities which enhanced the enhanced temperature contrast between the land and the sea induced by the expansion of Shanghai. During the advance of the sea breeze front inland, the Strong turbulent mixing and updraft induced by the sea -breeze front promoted the development of the urban boundary layervertical mixing of O_3, contributing to elevateelevating surfaced O_3 concentrationlevels at surface in Shanghai the city during the advance of the sea-breeze front inland (Figure 11a and b). When the sea -breeze matured around 17:00 LT, its transport effect reduced the surface O_3 concentration of the coastal cities (Figure 9c). However, this “transport effectremoval” was weakened because the sea -breeze near the surface was slowed affected bydue to the rough urban surface. Finally, surface O_3 of about ~10 μg m^{-3} was left compared to the scenario without cities (Figure 11c). In contrast to the onshore flow, the offshore flow transported high concentration of O_3 to the sea, which may be an important source of O_3 in the nocturnal residual layer. Influenced by the strong background southeast wind, the offshore flow was imperceptible during the day (Figure 9), but it can be enhanced by urban expansion (Figure 11c).

As for the lake -breeze, it was also enhanced by ~11-2 m s^{-1} after the establishment because of the larger temperature contrast resulting from the expansion of lakeside cities, just like the sea-breeze (Figure 11e and h).What’s more, And the life of the lake -breeze was extended to 17:00 LT (Figure 11f and i)) when the city exists. SinceBecause the lake -breeze circulation was conducive to the vertical mixing inof the boundary layer, and its onshore flow can transportedblow high concentration of O_3 from the lake to the city (Sect. 3.3.2), the urban O_3 concentration will eventually increase in the lakeside cities, with a maximum of 30 μg m^{-3} in Wuxi at 14:00 LT.

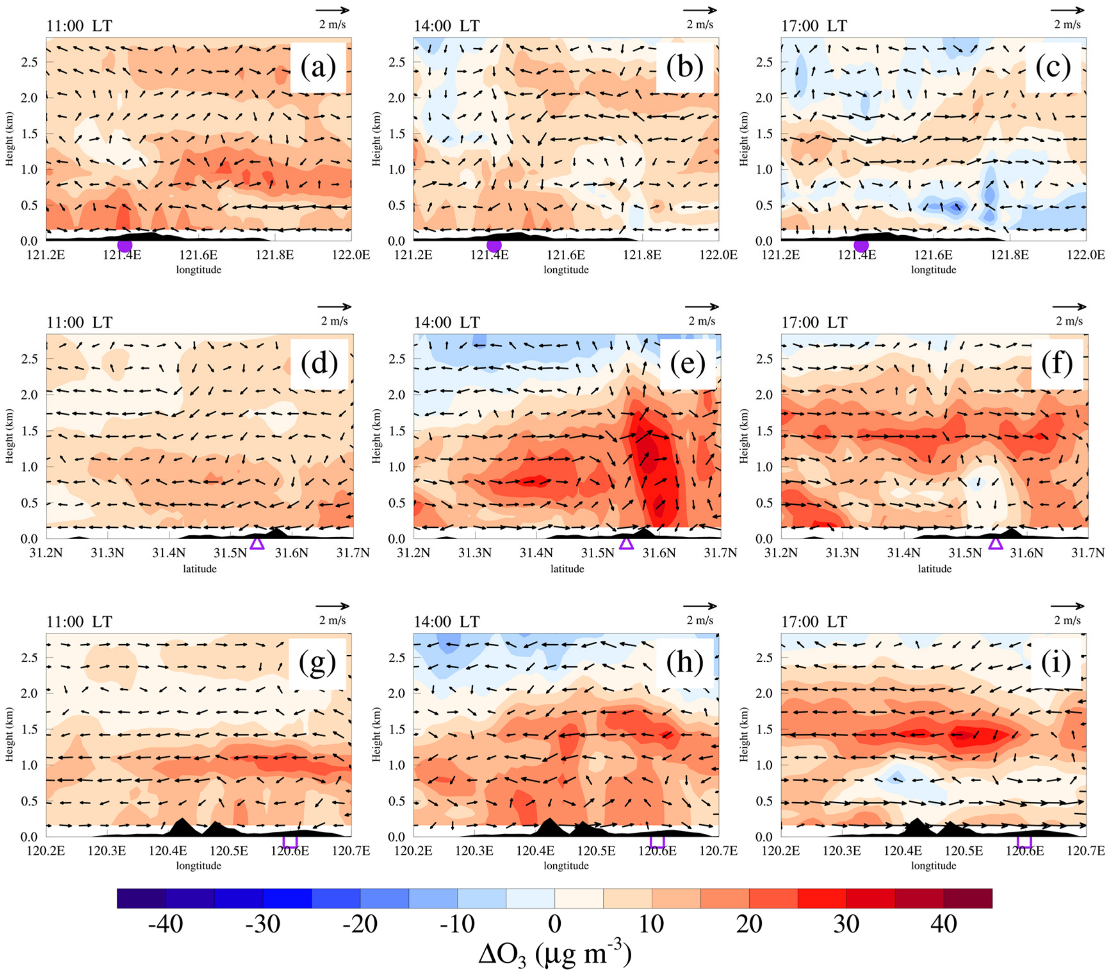
11:00 LT
14:00 LT
17:00 LT
2 m/s
(a)
(b)
(c)
(d)
(e)
(f)
(g)
(h)
(i)
Height (km)
longtitude
latitude
ΔO3 (μg m-3)

584

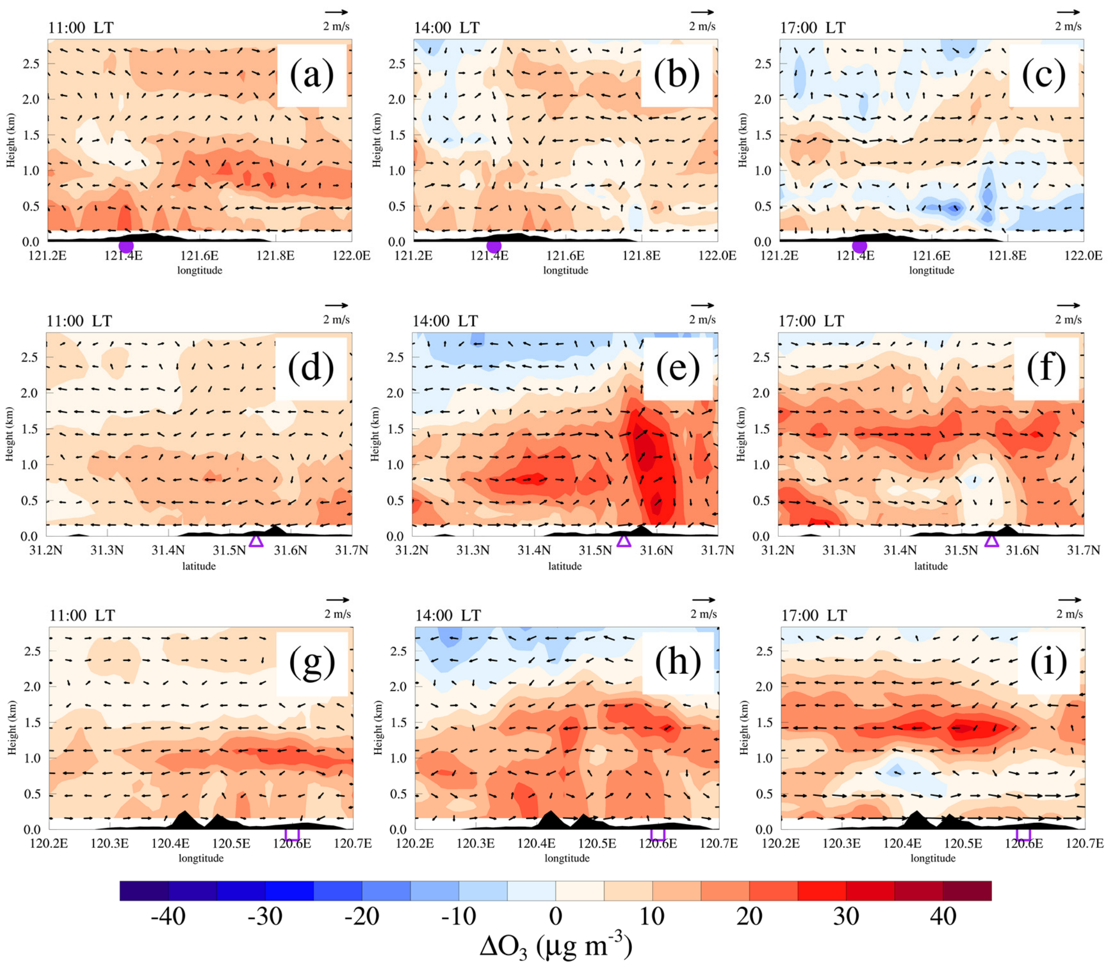

Figure 11. Same as Figure 9, but for the differences between MODIS_noAH and USGS_noAH (MODIS_noAH – USGS_noAH).

3.4.3 The mechanism of ~~land-surface forcing~~ land use modulating O_3

~~Land-surface forcing plays an important role in the evolution of O_3 by changing the local meteorology (meteorological factors and local circulations).~~ Changing land use~~land-surface forcing~~ from USGS to MODIS leads to an increase in T_2 by maximum 3 °C, an increase in PBLH by maximum 500 m and a decrease in WS_{10} by maximum 1.5 m s^{-1} in the YRD, which is comparable to those in the BTH region (Yu et al., 2012), the PRD region (Li et al., 2014) and the National Capital Region of India (Sati and Mohan, 2017). ~~And t~~These changes are particularly evident in and around cities as the biggest change in land use is related to urban expansion. The elevated air temperature is conducive to the photochemical production of O_3, and the well-developed boundary layer favors the vertical mixing of O_3 ~~(Figure 12).~~ These changes in meteorological factors~~,~~ ~~which~~ eventually increase~~s~~ the surface O_3 concentration ~~near the surface~~ by maximum 20 μg m^{-3} in the YRD.

Furthermore, This change magnitude in O_3 is consistent with the findings reported in Seoul (Ryu et al., 2013b) and Southern California (Li et al., 2019). lLocal circulations, including (the sea and the lake breezes,) are also influenced by urban expansion, which further alters O_3 in the vertical directionthe land-surface forcing., chiefly from the urban expansion as the most significant land-surface forcing in the YRD comes from urban expansion over the past few decades. For the coastal cities, like Shanghai, the larger temperature contrast caindueused byed by cities enhances the sea -breeze below 500 m. As the sea -breeze front moves inland, it can enhancesinduce stronger upward movementair flow that deepens the boundary layer, which is conductive to the mixing of O_3. in the boundary layer Thus, high O_3 concentration in the middle of boundary layer can be more easily transported to the surface. However, the movement of the sea -breeze is slowed due to the rough urban surface after the sea -breeze matures. The removal of the sea -breeze near the surface is then weakened and the surface O_3 increases by 10 μg m^{-3}. The similar response of the sea breezes to citiesurban expansion as well as its impact on O_3 has been also reported in the PRD region (You et al., 2019) and Paulo (Freitas et al., 2007). For the lakeside cities, like Wuxi and Suzhou, the lifetime of the lake breezes is extended to the afternoon due to the existence ofexpansion of citiesthe city. The offshore flow of the lake -breeze transports high O_3 concentration in the middle of the boundary layer from the land to the lake, while the onshore flow brings the O_3 back to the land, which accelerates the vertical mixing of O_3 and can increases the surface O_3 by even 30 μg m^{-3}. Thus, hHigh surface O_3 usually appears when the lake breezes is have been established. Thised wascan also be observed in the Greater Toronto Area (Wentworth et al., 2015) and the Lake Michigan (Abdi-Oskouei et al., 2020).

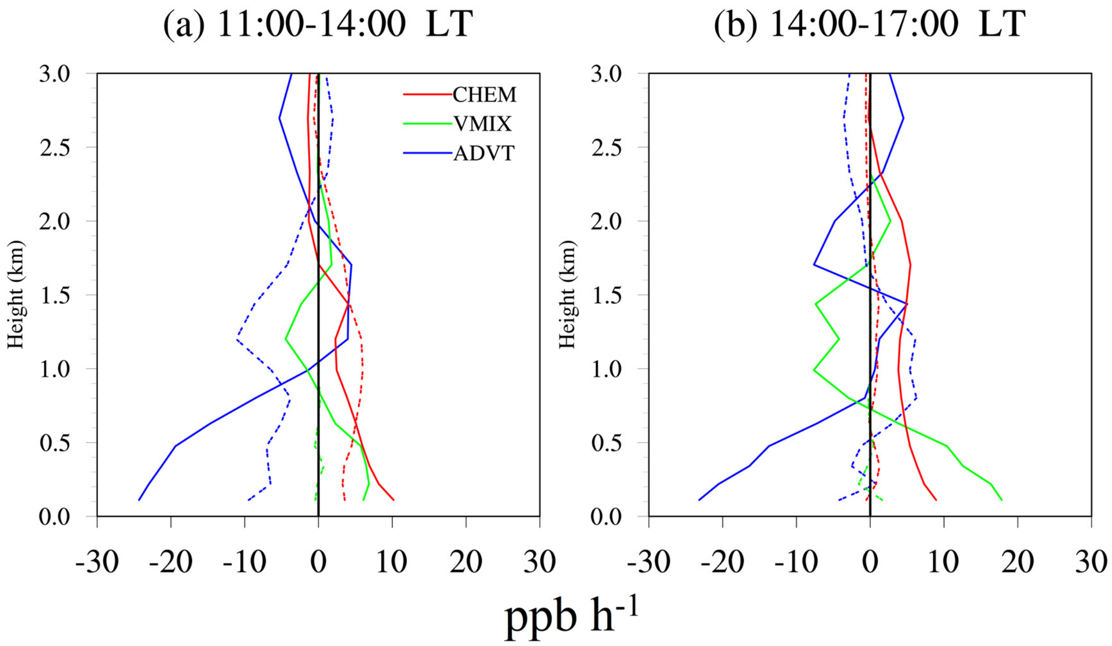

~~**Figure 12.** Vertical profiles of the changes in individual processes between MODIS_noAH and USGS_noAH (MODIS_noAH – USGS_noAH) at (a) 11:00-14:00 LT and (b) 14:00-17:00 LT over Shanghai (solid lines) and Wuxi (dashed lines). CHEM (in red), VMIX (in green) and ADVT (in blue) represent gas-phase chemical reactions, turbulent mixing and advection transport, respectively.~~

3.5 Impacts of anthropogenic heat on meteorology and O_3

3.5.1 Horizontal changes

Compared with land use~~land-surface forcing~~, the changes caused by AH are much smaller (Figure ~~13~~12). Furthermore, these changes ~~in meteorology and O_3~~ are effective~~mainly occur~~ in and around cities as ~~there are more AH emissions in~~ they usually have large AH flux density ~~these areas~~ (Figure 3). By adding more surface sensible heat into the atmosphere, the AH fluxes leaded to an increase in T_2 of 0.2 °C in urban areas, with the typical value of 0.42 °C in Shanghai (Figure 12a-d). Vertical air movement in the boundary layer was then enhanced by the warming of T_2, and the PBLH will increase as well. According to the simulations, the PBLH increased by ~75 m in the urban areas (Figure 12e-h). Contrary to the decrease in WS_{10} caused by urban expansion, WS_{10} increased by ~0.3 m s^{-1} in the urban areas when AH fluxes were taken into account (Figure 12i-l). This is ascribed to the strengthened urban breeze circulations caused by the AH fluxes, which is conducive to the transmission of momentum from the upper layer to the surface. With regard to surface O_3 concentration, it increased by ~4 μg m^{-3} in the simulation with adding AH. In particular, the increases in T_2, PBLH, WS_{10} and O_3 seemed to be clearer after sunset as the solar shortwave radiation disappeared. Surface O_3 concentration increased in the urban areas by about 4 μg m^{-3} in the simulation with adding AH, and this phenomenon was clearer after sunset (Figure 13d). By adding more surface sensible heat into the atmosphere, the AH fluxes can lead to an increase in T_2 of 0.2 °C during the day, with the typical value of 0.42 °C in Shanghai. Vertical air movement in the boundary layer can be enhanced by the warming up of the surface air temperature, thereby the PBLH will increase as well. According to the simulations, the PBLH increased by about 75 m in the urban areas. With regards to WS_{10}, it increased by about 0.3 m s^{-1} in the urban areas, which is contrary to the decrease in WS_{10} caused by land-surface forcing (Sect. 3.4.1). This is ascribed to the strengthened urban-breeze circulations induced by the AH fluxes, which is mentioned in previous studies (Ryu et al., 2013a, b; Xie et al., 2016a, b).

654

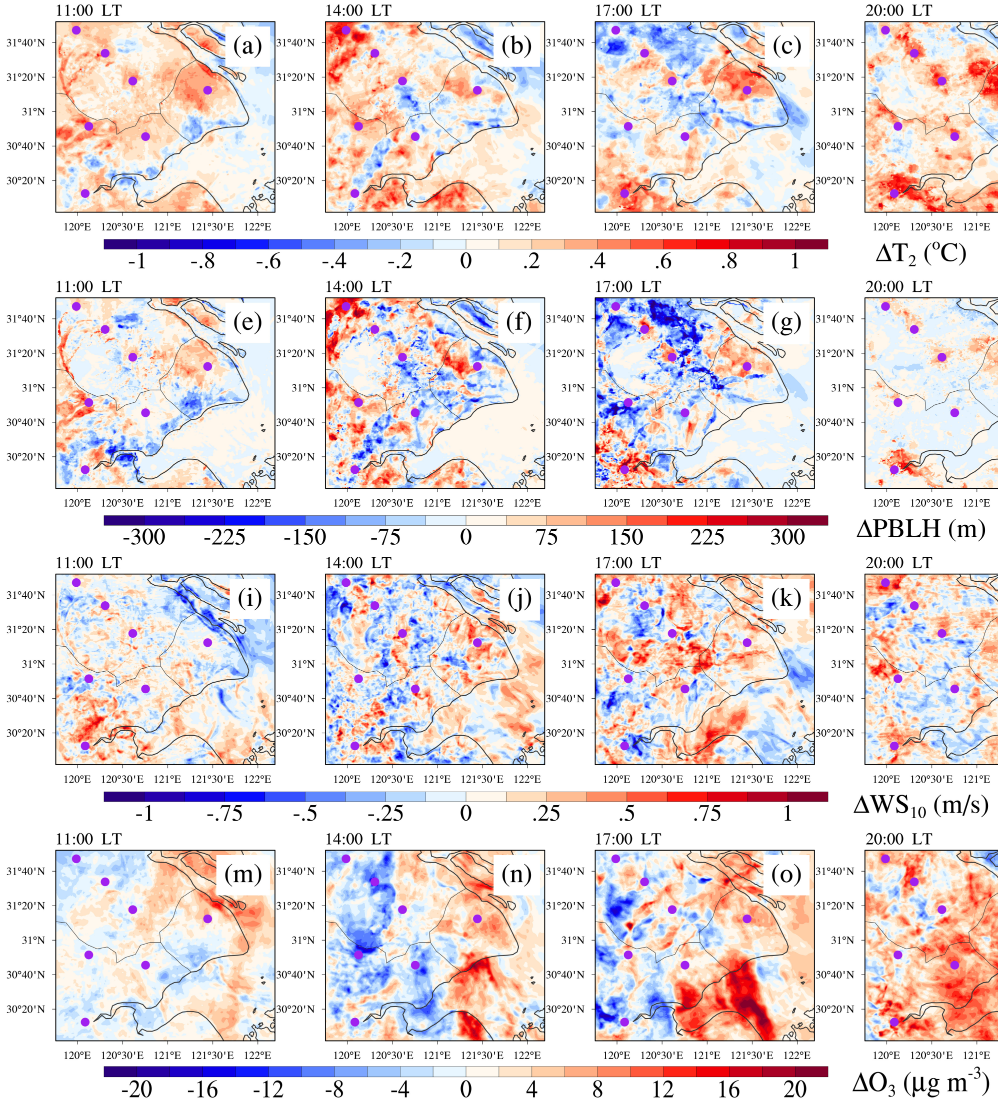

11:00 LT
14:00 LT
17:00 LT
20:00 LT
(a) (b) (c) (d)
ΔT2 (°C)
-1 -.8 -.6 -.4 -.2 0 .2 .4 .6 .8 1
(e) (f) (g) (h)
ΔPBLH (m)
-300 -225 -150 -75 0 75 150 225 300
(i) (j) (k) (l)
ΔWS10 (m/s)
-1 -.75 -.5 -.25 0 .25 .5 .75 1
(m) (n) (o) (p)
ΔO3 (μg m-3)
-20 -16 -12 -8 -4 0 4 8 12 16 20
31°40'N
31°20'N
31°N
30°40'N
30°20'N
120°E
120°30'E
121°E
121°30'E
122°E

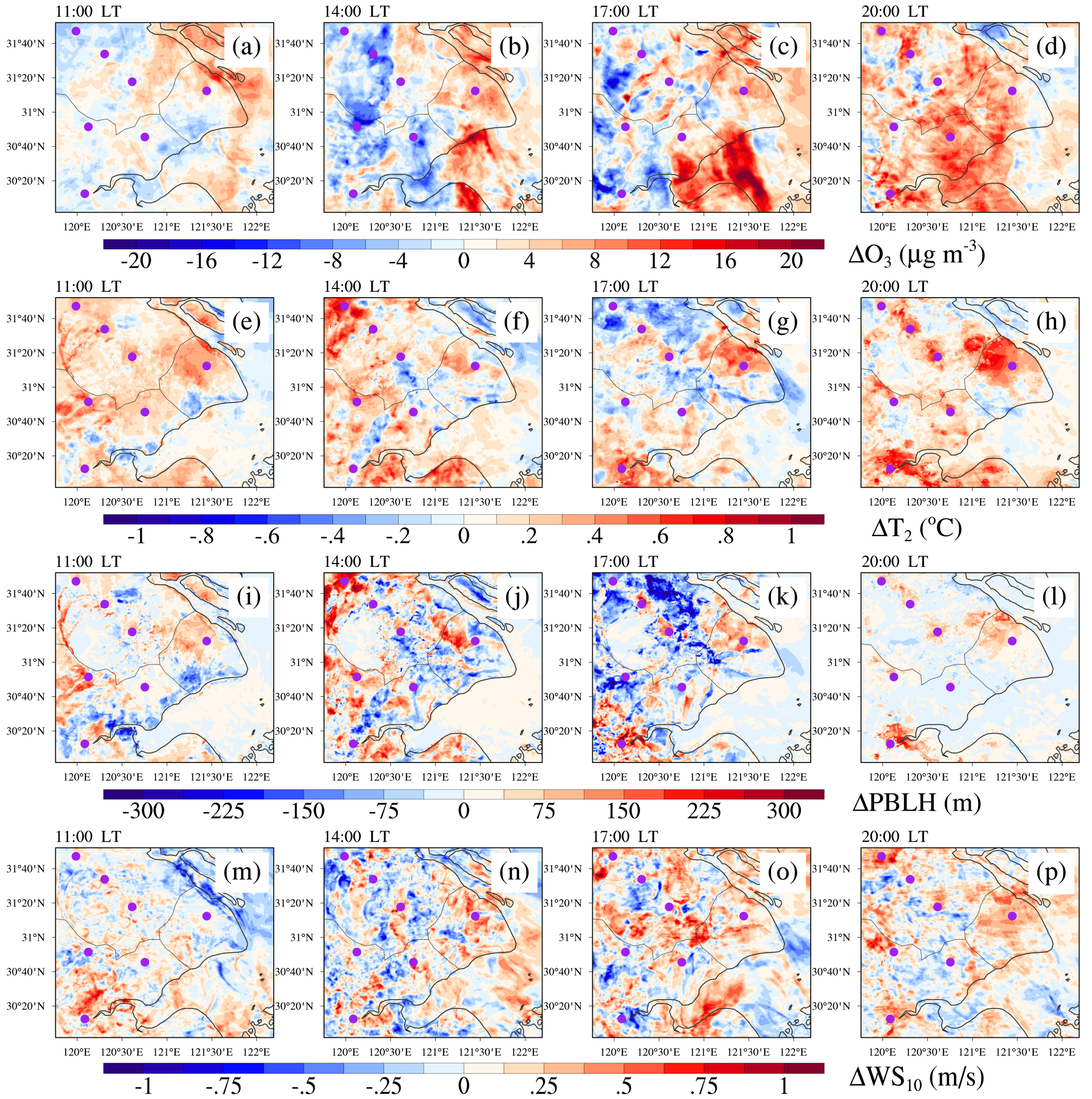

Figure ~~13~~12. Same as Figure 10, but for the differences between MODIS_~~with~~AH and MODIS_noAH (MODIS_~~with~~AH – MODIS_noAH).

3.5.2 Vertical changes

The phenomenon that cities are almost always warmer than their surroundings is widely known as the urban heat island (UHI), and the difference between the urban and the rural surface energy balance can further induce~~itiate~~ the urban heat island~~UHI~~ circulation (UHIC). It is clearly seen that an enhanced UHI~~ circulation~~C driven by AH appeared in the megacity Shanghai around 14:00 LT (Figure ~~14b~~13b). This circulation extended horizontally 20-30 km from the city center to the urban edge, and vertically to ~~nearly ~~~2 km from the ground to the top of the urban boundary layer. In this case~~Under this condition~~, there was a small increase (4~6 μg m^{-3}) in surface O_3~~ concentrations in the low boundary layer~~. However, for the lakeside cities, the enhanced UHI~~ circulation~~C was not perceptible~~visibly noticed~~.~~,~~ And t~~and t~~he O_3 concentration in urban areas was reduced on average, with a maximum of 16 μg m^{-3} in Wuxi around 14:00 LT (Figure ~~14e~~13e). The decrease in O_3~~e lower O_3 concentration~~ may be related to~~affected by~~ the increased wind ~~on the lake~~ (Figure ~~13~~12i-k), which was beneficial to the diffusion and dilution of O_3~~processes~~. Furthermore, ~~it seems that~~ AH has a limited effect on ~~local circulations, regardless of~~ the sea and~~or~~ lake breeze as, ~~–~~ it cannot affect any branch of the two as significantly as the urban expansion. ~~though it play an important role in the urban-breeze circulations. In our simulation cases, AH does not continuously and significantly affect any branch of the local circulations like the land-surface forcing.~~

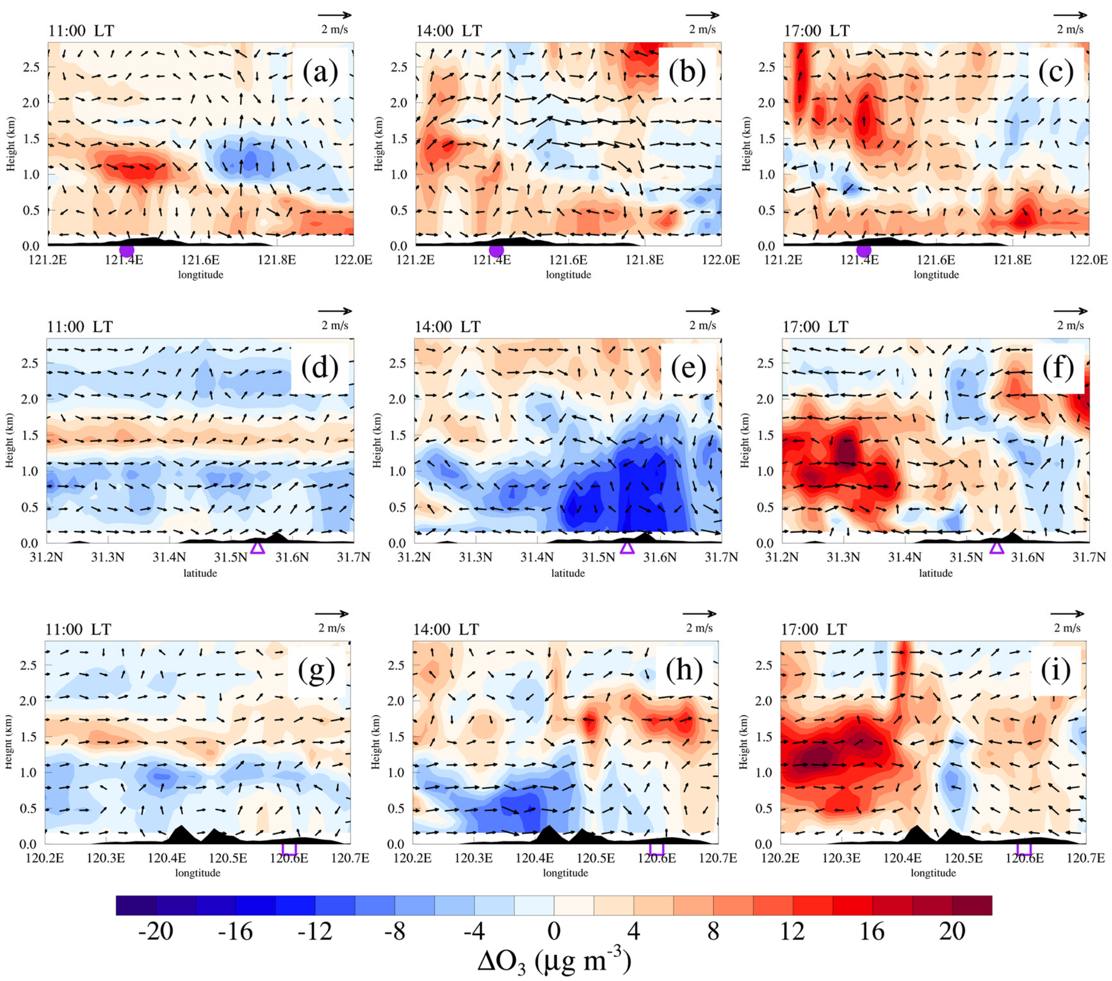

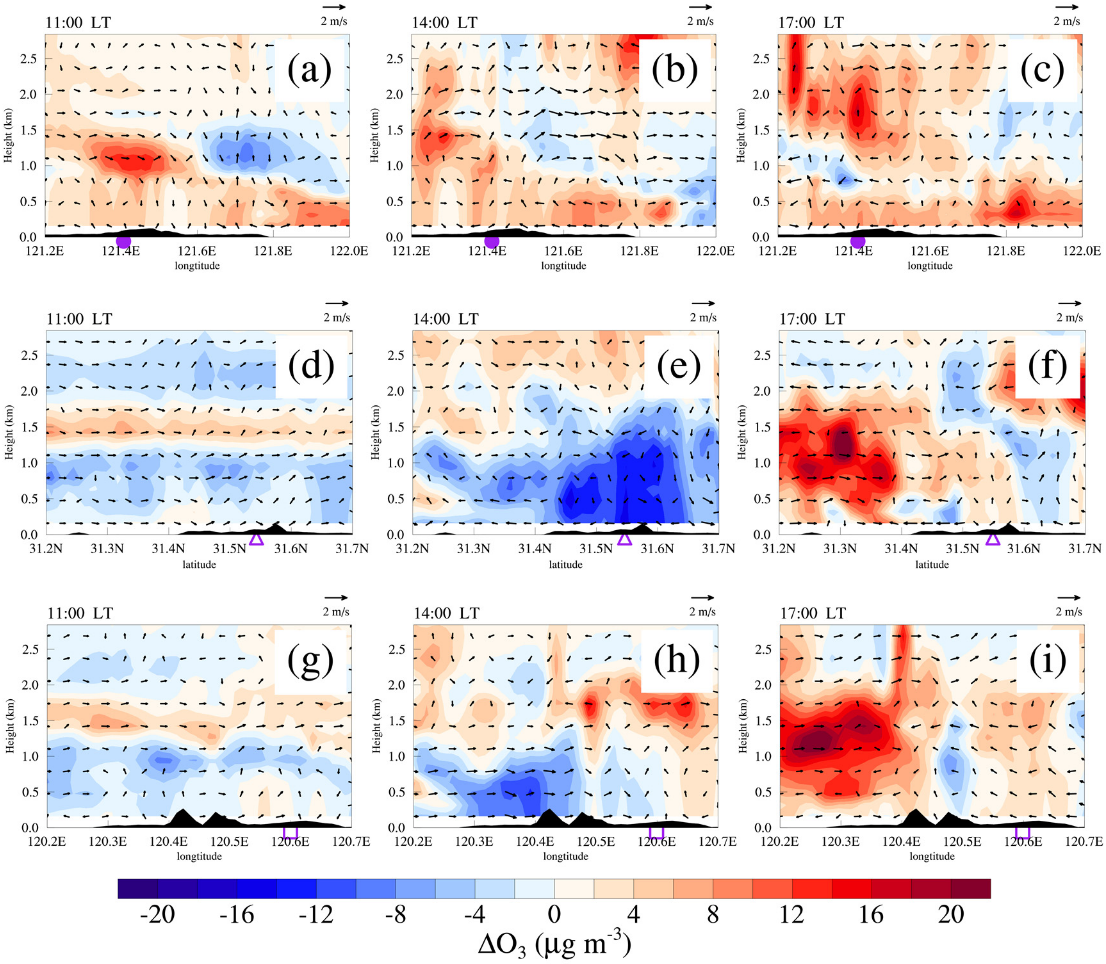

Figure 1413. Same as Figure 89, but for the differences between MODIS_withAH and MODIS_noAH (MODIS_withAH – MODIS_noAH).

3.5.3 The mechanism of anthropogenic heat modulating O_3

AH and land-surface forcingland use play different roles in meteorology and O_3. AH allows the atmosphere to reserve more energy via the additional sensible heat fluxes, which increases T_2 by ~about 0.2 °C. Higher temperature is conducive to the development of the convective boundary layer and can induces stronger upward air movement to the development of the convective boundary layer, risingwhich rises the PBLH by ~about 75 m. In the convective boundary layer, the atmosphere is associated with turbulent motions, and is unstable. Together with the enhanced urban -breeze causedcirculations enhanced by AH, WS_{10} can increases by 0.3 m s^{-1}. These findings are comparable to the values estimated in other cities all around the world, such as Philadelphia in the United States (Fan and Sailor, 2005), Winnipeg in Canada (Ferguson and Woodbury, 2007) and, Berlin in German

(Menberg et al., 2013)~~ and Tokyo in Japan (Dhakal and Hanaki, 2002)~~. These changes in meteorological factors eventually lead to an increase in surface O_3 by ~4 μg m^{-3}. It is noteworthy that ~~the abovementioned changes mainly appear in large cities and their surrounding areas, where AH emission centers are located~~the effects of AH are usually clearer at night in urban areas~~. And these changes eventually caused an increase in surface O_3 concentration by about 4 μg m^{-3}~~. In addition~~Additionally~~, though AH ~~can~~ plays an important role in urban ~~-~~breeze circulations, it may not be powerful enough to affect the local circulations such as the sea and the lake breezes~~s~~.

4 Summary and conclusions

Land use change via ~~Land-surface forcing related to the u~~urban expansion ~~and~~ and the increase of AH are important manifestations of urbanization~~AH release from human activities can change the meteorology (meteorological factors and local circulations)~~. They can alter the regional meteorology, and~~and~~ thereby affect O_3 ~~air quality~~concentrations in and around cities. In this study, the YRD region, a highly urbanized coastal ~~place~~ area with sever O_3 pollution~~ and complex geography~~, is selected to discuss this issue. Firstly, ~~we briefly describe the general~~the basic characteristics of O_3 pollution in the YRD are investigated based on the surface observations. Secondly, ~~we simulate~~ a representative case is selected to further study using WRF-C~~c~~hem model, and ~~evaluate~~ the model performance is evaluated by comparing with the observations~~al data~~. Finally, the response of ~~meteorology as well as~~ O_3 to changes in meteorology caused by urban expansion~~land-surface forcing~~ and AH are discussed~~investigated~~ ~~from the model results~~via the model inter-comparisons. The main findings are listed as below:

(1) Regional O_3 pollution occurs frequently in the YRD (~~~~~26 times per year). ~~Like other regions, t~~These O_3 pollution episodes mainly occur ~~in warm season (April to October)~~ in~~under~~ calm conditions characterized by high temperature (over 20 °C), low relative humidity (less than 80%), light wind (less than 3 m s^{-1}) and shallow cloud cover (less than 5 okta). In this case, the sea and lake breezes ~~local circulations induced by thermal differentiation~~ tend to develop and ~~will~~ have an important impact on the distribution of O_3 in this region.

(2) By updating the land ~~-~~use data from USGS to MODIS, we find an increase in T_2 by maximum 3 °C, an increase in PBLH by maximum 500 m and a decrease in WS_{10} by maximum 1.5 m s^{-1} in the YRD~~, which is comparable to those in the BTH region (Yu et al., 2012), the PRD region~~

(Li et al., 2014) and the National Capital Region of India (Sati and Mohan, 2017). The higher temperature and PBLH elevate surface O_3 concentrationthe O_3 level by maximum 20 μg m^{-3} via the stronger photochemical reactions and the vertical mixing processes, respectively. These changes are mainly attributed to urban expansion associated with urbanization. For changes in local circulationsFurthermore, the sea -breeze below 500 m is enhanced due to larger temperature contrast induced by the urban expansion of coastal cities. Nevertheless, . During the advance of the sea-breeze front inland, the upward air flow in front of the front is conducive to the vertical mixing of O_3. When the sea-breeze is well formed in the late afternoon, further progression inland of the sea breeze in the afternoon can beis stalled on account of the rough urban surface, reducing the transmission of O_3 from the coast to the land.. The transport of high O_3 from coastal to the inland areas is weakened and thereby O_3 can be 10 μg m^{-3} higher in the case with cities than without. The similar results have been also reported in the Paulo (Freitas et al., 2007) and the PRD region (You et al., 2019). With respect to the lake breezesThe expansion of lakeside cities extends ,the its lifetime of the lake breeze will be extended from the noon to – the afternoon because of the urban expansion. Since the net effect of the lake -breeze canis to accelerate the vertical mixing of O_3 in the boundary layer, the surface O_3 in lakeside cities can– increase by evenas much as 30 μμg m^{-3} influenced by the lake-breeze. Similar phenomenon also be observed in the Greater Toronto Area (Wentworth et al., 2015) and the Lake Michigan (Abdi-Oskouei et al., 2020).

(3) The changes caused by AH are different from land-surface forcing.When the AH fluxes are taken into account, T_2, PBLH, WS_{10} and O_3 will increase by about 0.2 °C, 75 m, 0.3 m s^{-1} and 4 μg m^{-3} in and around cities. These changes are relatively small compared to urban expansion, and mainly appear around the cities where the there are large AH fluxes are usually large emissions.. Through regulating the land-atmosphere heat fluxes, O_3, T_2, PBLH and WS_{10} increases by about 4 μg m^{-3}, 0.2 °C, 75 m and 0.3 m s^{-1} under the effect of the additional sensible heat fluxes induced by AH. The magnitudes of these changes are consistent with the values estimated in other cities all around the world, including Philadelphia in the United States (Fan and Sailor, 2005), Winnipeg in Canada (Ferguson and Woodbury, 2007), Tokyo in Japan (Dhakal and Hanaki, 2002) and Berlin in German (Menberg et al., 2013). AdditionallyIn addition, unlike the urban expansion, our results show that AH may have a quite limited impact on local circulations, such as the sea and the lake breezes. ButBut the urban -breeze circulations are found to be sensitive to AH inputs.in and around

~~big cities are sensitive to AH inputs, which can further affect the urban air pollutants.~~

~~Estimating the impacts of land-surface forcing and AH on urban climate and air quality is a complex but necessary issue as these two are important manifestations of urbanization.~~Studying the impacts of land use and AH forced by human activities on urban environment is fundamental in improving the urban air quality. Although this~~our~~ study only focuses on the YRD region, most of the results can be supported by previous studies that conducted in other region around the world. As more and more city clusters composed of large and medium-sized cities are being built. This~~Thus, our~~ work can~~may~~ provide valuable insight into the formation of O_3 pollution in those rapidly developing regions with unique geographical features.

Data Availability Statement.

Air quality monitoring data were acquired from a mirror of data from the official NEMC real-time publishing platform (https://quotsoft.net/air/). Meteorological data were issued by the NCDC (ftp://ftp.ncdc.noaa.gov/pub/data/noaa/isd-lite/). The FNL meteorological data were acquired from NCEP (https://doi.org/10.5065/D6M043C6/). These data can be downloaded for free as long as you agree to the official instructions.

Author contributions.

CZ and MX had the original ideas, designed the research, collected the data and prepared the original draft. CZ did the numerical simulations and carried out the data analysis. MX acquired financial support for the project leading to this publication.

Acknowledgements.

This work was supported by the National Key Research and Development Program of China (2018YFC0213502, 2018YFC1506404). We are grateful to MEPC for the air quality monitoring data, to NCDC for the meteorological data, to NCEP for global final analysis fields and to Tsinghua University for the MEIC inventories. The numerical calculations have been done on the Blade cluster system in the High Performance Computing and Massive Data Center (HPC&MDC) of School of Atmospheric Sciences, Nanjing University. We also thank the constructive comments and suggestions from the anonymous reviewers.

References

Abdi-Oskouei, M., Carmichael, G., Christiansen, M., Ferrada, G., Roozitalab, B., Sobhani, N., Wade, K., Czarnetzki, A., Pierce, R. B., Wagner, T., and Stanier, C.: Sensitivity of Meteorological Skill to Selection of WRF-Chem Physical Parameterizations and Impact on Ozone Prediction During the Lake Michigan Ozone Study (LMOS), J Geophys Res-Atmos, 125, 2020.

Bergin, M. S., West, J. J., Keating, T. J., and Russell, A. G.: Regional atmospheric pollution and transboundary air quality management, Annu. Rev. Environ. Resour., 30, 1-37, 10.1146/annurev.energy.30.050504.144138, 2005.

Blaylock, B. K., Horel, J. D., and Crosman, E. T.: Impact of Lake Breezes on Summer Ozone Concentrations in the Salt Lake Valley, Journal of Applied Meteorology and Climatology, 56, 353-370, 2017.

Buchholz, S., Junk, J., Krein, A., Heinemann, G., and Hoffmann, L.: Air pollution characteristics associated with mesoscale atmospheric patterns in northwest continental Europe, Atmospheric Environment, 44, 5183-5190, 10.1016/j.atmosenv.2010.08.053, 2010.

Chameides, W., and Walker, J. C. G.: A photochemical theory of tropospheric ozone, Journal of Geophysical Research, 78, 8751-8760, 10.1029/JC078i036p08751, 1973.

Chen, F., and Dudhia, J.: Coupling an advanced land surface-hydrology model with the Penn State-NCAR MM5 modeling system. Part II: Preliminary model validation, Monthly Weather Review, 129, 587-604, 2001.

Chen, S. H., and Sun, W. Y.: A one-dimensional time dependent cloud model, J Meteorol Soc Jpn, 80, 99-118, 2002.

Crosman, E. T., and Horel, J. D.: Sea and Lake Breezes: A Review of Numerical Studies, Boundary-Layer Meteorology, 137, 1-29, 10.1007/s10546-010-9517-9, 2010.

~~Dhakal, S., and Hanaki, K.: Improvement of urban thermal environment by managing heat discharge sources and surface modification in Tokyo, Energ Buildings, 34, 13-23, 2002.~~

Ding, A., Wang, T., Zhao, M., Wang, T., and Li, Z.: Simulation of sea-land breezes and a discussion of their implications on the transport of air pollution during a multi-day ozone episode in the Pearl River Delta of China, Atmospheric Environment, 38, 6737-6750, 10.1016/j.atmosenv.2004.09.017, 2004.

Ding, A. J., Fu, C. B., Yang, X. Q., Sun, J. N., Zheng, L. F., Xie, Y. N., Herrmann, E., Nie, W., Petäjä, T., Kerminen, V. M., and Kulmala, M.: Ozone and fine particle in the western Yangtze River Delta: an overview of 1 yr data at the SORPES station, Atmospheric Chemistry and Physics, 13, 5813-5830, 10.5194/acp-13-5813-2013, 2013.

Fan, H. L., and Sailor, D. J.: Modeling the impacts of anthropogenic heating on the urban climate of Philadelphia: a comparison of implementations in two PBL schemes, Atmospheric Environment, 39, 73-84, 2005.

Fast, J. D., Gustafson, W. I., Easter, R. C., Zaveri, R. A., Barnard, J. C., Chapman, E. G., Grell, G. A., and Peckham, S. E.: Evolution of ozone, particulates, and aerosol direct radiative forcing in the vicinity of Houston using a fully coupled meteorology-chemistry-aerosol model, J Geophys Res-Atmos, 111, 2006.

Ferguson, G., and Woodbury, A. D.: Urban heat island in the subsurface, Geophysical Research Letters, 34, 2007.

Flanner, M. G.: Integrating anthropogenic heat flux with global climate models, Geophysical Research Letters, 36, n/a-n/a, 10.1029/2008gl036465, 2009.

Freitas, E. D., Rozoff, C. M., Cotton, W. R., and Dias, P. L. S.: Interactions of an urban heat island and sea-breeze circulations during winter over the metropolitan area of Sao Paulo, Brazil, Boundary-Layer Meteorology, 122, 43-65, 2007.

Friedl, M. A., Sulla-Menashe, D., Tan, B., Schneider, A., Ramankutty, N., Sibley, A., and Huang, X.: MODIS Collection 5 global land cover: Algorithm refinements and characterization of new datasets, Remote Sensing of Environment, 114, 168-182, 10.1016/j.rse.2009.08.016, 2010.

Fu, Y. and Liao, H.: Impacts of land use and land cover changes on biogenic emissions of volatile organic compounds in China from the late 1980s to the mid-2000s: implications for tropospheric ozone and secondary organic aerosol, Tellus B: Chemical and Physical Meteorology, 66, 10.3402/tellusb.v66.24987, 2014.

Gao, D., Xie, M., Chen, X., Wang, T. J., Liu, J., Xu, Q., Mu, X. Y., Chen, F., Li, S., Zhuang, B. L., Li, M. M., Zhao, M., and Ren, J. Y.: Systematic classification of circulation patterns and integrated analysis of their effects on different ozone pollution levels in the Yangtze River Delta Region, China, Atmospheric Environment, 242, 2020.

Gong, P., Liu, H., Zhang, M., Li, C., Wang, J., Huang, H., Clinton, N., Ji, L., Li, W., Bai, Y., Chen, B., Xu, B., Zhu, Z., Yuan, C., Ping Suen, H., Guo, J., Xu, N., Li, W., Zhao, Y., Yang, J., Yu, C., Wang, X., Fu, H., Yu, L., Dronova, I., Hui, F., Cheng, X., Shi, X., Xiao, F., Liu, Q., and Song, L.: Stable classification with limited sample: transferring a 30-m resolution sample set collected in 2015 to mapping 10-m resolution global land cover in 2017, Science Bulletin, 64, 370-373, 10.1016/j.scib.2019.03.002, 2019.

Grell, G. A., and Dévényi, D.: A generalized approach to parameterizing convection combining ensemble and data assimilation techniques, Geophysical Research Letters, 29, 38-31-38-34, 10.1029/2002gl015311, 2002.

Grell, G. A., Peckham, S. E., Schmitz, R., McKeen, S. A., Frost, G., Skamarock, W. C., and Eder, B.: Fully coupled “online” chemistry within the WRF model, Atmospheric Environment, 39, 6957-6975, 10.1016/j.atmosenv.2005.04.027, 2005.

Guenther, A., Karl, T., Harley, P., Wiedinmyer, C., Palmer, P. I., and Geron, C.: Estimates of global terrestrial isoprene emissions using MEGAN (Model of Emissions of Gases and Aerosols from Nature), Atmospheric Chemistry and Physics, 6, 3181-3210, 2006.

Hong, S. Y., Noh, Y., and Dudhia, J.: A new vertical diffusion package with an explicit treatment of entrainment processes, Monthly Weather Review, 134, 2318-2341, 2006.

Hu, J., Li, Y., Zhao, T., Liu, J., Hu, X.-M., Liu, D., Jiang, Y., Xu, J., and Chang, L.: An important mechanism of regional O₃ transport for summer smog over the Yangtze River Delta in eastern China, Atmospheric Chemistry and Physics, 18, 16239-16251, 10.5194/acp-18-16239-2018, 2018.

Jacob, D. J., and Winner, D. A.: Effect of climate change on air quality, Atmospheric Environment, 43, 51-63, 10.1016/j.atmosenv.2008.09.051, 2009.

Jerrett, M., Burnett, R. T., Pope, C. A., Ito, K., Thurston, G., Krewski, D., Shi, Y. L., Calle, E., and Thun, M.: Long-Term Ozone Exposure and Mortality., New Engl J Med, 360, 1085-1095, 2009.

Jiang, X., Wiedinmyer, C., Chen, F., Yang, Z.-L., and Lo, J. C.-F.: Predicted impacts of climate and land use change on surface ozone in the Houston, Texas, area, Journal of Geophysical Research, 113, 10.1029/2008jd009820, 2008.

Jimenez, P. A., and Dudhia, J.: Improving the Representation of Resolved and Unresolved Topographic Effects on Surface Wind in the WRF Model, Journal of Applied Meteorology and Climatology, 51, 300-316, 2012.

Kim, H.-J., and Wang, B.: Sensitivity of the WRF model simulation of the East Asian summer monsoon in 1993 to shortwave radiation schemes and ozone absorption, Asia-Pacific Journal of Atmospheric Sciences, 47, 167-180, 10.1007/s13143-011-0006-y, 2011.

Lennartson, G. J., and Schwartz, M. D.: The lake breeze-ground-level ozone connection in eastern Wisconsin: A climatological perspective, International Journal of Climatology, 22, 1347-1364, 2002.

Li, K., Jacob, D. J., Shen, L., Lu, X., De Smedt, I., and Liao, H.: Increases in surface ozone pollution in China from 2013 to 2019: anthropogenic and meteorological influences, Atmospheric Chemistry and Physics, 20, 11423-11433, 10.5194/acp-20-11423-2020, 2020.

Li, M., Song, Y., Huang, X., Li, J., Mao, Y., Zhu, T., Cai, X., and Liu, B.: Improving mesoscale modeling using satellite-derived land surface parameters in the Pearl River Delta region, China, Journal of Geophysical Research: Atmospheres, 119, 6325-6346, 10.1002/2014jd021871, 2014.

Li, M., Wang, T., Xie, M., Zhuang, B., Li, S., Han, Y., Song, Y., and Cheng, N.: Improved meteorology and ozone air quality simulations using MODIS land surface parameters in the Yangtze River Delta urban cluster, China, Journal of Geophysical Research: Atmospheres, 122, 3116-3140, 10.1002/2016jd026182, 2017.

Li, Y., Zhang, J., Sailor, D. J., and Ban-Weiss, G. A.: Effects of urbanization on regional meteorology and air quality in Southern California, Atmospheric Chemistry and Physics, 19, 4439-4457, 10.5194/acp-19-4439-2019, 2019.

Li, K., Jacob, D. J., Shen, L., Lu, X., De Smedt, I., and Liao, H.: Increases in surface ozone pollution in China from 2013 to 2019: anthropogenic and meteorological influences, Atmospheric Chemistry and Physics, 20, 11423-11433, 10.5194/acp-20-11423-2020, 2020.

Liao, Z., Gao, M., Sun, J., and Fan, S.: The impact of synoptic circulation on air quality and pollution-related human health in the Yangtze River Delta region, Sci Total Environ, 607-608, 838-846, 10.1016/j.scitotenv.2017.07.031, 2017.

Lin, C. H., Lai, C. H., Wu, Y. L., Lin, P. H., and Lai, H. C.: Impact of sea breeze air masses laden with ozone on inland surface ozone concentrations: A case study of the northern coast of Taiwan, J Geophys Res-Atmos, 112, 2007.

Liu, M., and Tian, H.: China's land cover and land use change from 1700 to 2005: Estimations from high-resolution satellite data and historical archives, Global Biogeochemical Cycles, 24, n/a-n/a, 10.1029/2009gb003687, 2010.

Loveland, T. R., Reed, B. C., Brown, J. F., Ohlen, D. O., Zhu, Z., Yang, L., and Merchant, J. W.: Development of a global land cover characteristics database and IGBP DISCover from 1 km AVHRR data, International Journal of Remote Sensing, 21, 1303-1330, 10.1080/014311600210191, 2000.

Lu, X., Hong, J., Zhang, L., Cooper, O. R., Schultz, M. G., Xu, X., Wang, T., Gao, M., Zhao, Y., and Zhang, Y.: Severe Surface Ozone Pollution in China: A Global Perspective, Environmental Science & Technology Letters, 5, 487-494, 10.1021/acs.estlett.8b00366, 2018.

Mavrakou, T., Philippopoulos, K., and Deligiorgi, D.: The impact of sea breeze under different synoptic patterns on air pollution within Athens basin, Science of the Total Environment, 433, 31-43, 2012.

Menberg, K., Bayer, P., Zosseder, K., Rumohr, S., and Blum, P.: Subsurface urban heat islands in German cities, Sci Total Environ, 442, 123-133, 10.1016/j.scitotenv.2012.10.043, 2013.

Miao, Y., Hu, X.-M., Liu, S., Qian, T., Xue, M., Zheng, Y., and Wang, S.: Seasonal variation of local atmospheric circulations and boundary layer structure in the Beijing-Tianjin-Hebei region and implications for air quality, Journal of Advances in Modeling Earth Systems, 7, 1602-1626, 10.1002/2015ms000522, 2015.

Mills, G., Hayes, F., Simpson, D., Emberson, L., Norris, D., Harmens, H., and Buker, P.: Evidence of widespread effects of ozone on crops and (semi-)natural vegetation in Europe (1990-2006) in relation to AOT40-and flux-based risk maps, Glob. Change Biol., 17, 592-613, 10.1111/j.1365-2486.2010.02217.x, 2011.

Mlawer, E. J., Taubman, S. J., Brown, P. D., Iacono, M. J., and Clough, S. A.: Radiative transfer for inhomogeneous atmospheres: RRTM, a validated correlated-k model for the longwave, Journal of Geophysical Research: Atmospheres, 102, 16663-16682, 10.1029/97jd00237, 1997.

Oke, T. R.; Mills, G.; Christen, A.; Voogt, J. A. Urban Climates; Cambridge University Press: Cambridge, 2017.

Park, R. J., Hong, S. K., Kwon, H. A., Kim, S., Guenther, A., Woo, J. H., and Loughner, C. P.: An evaluation of ozone dry deposition simulations in East Asia, Atmospheric Chemistry and Physics, 14, 7929-7940, 10.5194/acp-14-7929-2014, 2014.

Ryu, Y. H., Baik, J. J., Kwak, K. H., Kim, S., and Moon, N.: Impacts of urban land-surface forcing on ozone air quality in the Seoul metropolitan area, Atmospheric Chemistry and Physics, 13, 2177-2194, 10.5194/acp-13-2177-2013, 2013b.

Ryu, Y.-H., Baik, J.-J., and Lee, S.-H.: Effects of anthropogenic heat on ozone air quality in a megacity, Atmospheric Environment, 80, 20-30, 10.1016/j.atmosenv.2013.07.053, 2013a.

Sailor, D. J.: A review of methods for estimating anthropogenic heat and moisture emissions in the urban environment, International Journal of Climatology, 31, 189-199, 10.1002/joc.2106, 2011.

Sati, A. P., and Mohan, M.: The impact of urbanization during half a century on surface meteorology based on WRF model simulations over National Capital Region, India, Theoretical and Applied Climatology, 134, 309-323, 2017.

Schell, B., Ackermann, I. J., Hass, H., Binkowski, F. S., and Ebel, A.: Modeling the formation of secondary organic aerosol within a comprehensive air quality model system, J Geophys Res-Atmos, 106, 28275-28293, 2001.

Shao, M., Tang, X. Y., Zhang, Y. H., and Li, W. J.: City clusters in China: air and surface water pollution, Front Ecol Environ, 4, 353-361, 2006.

Sills, D. M. L., Brook, J. R., Levy, I., Makar, P. A., Zhang, J., and Taylor, P. A.: Lake breezes in the southern Great Lakes region and their influence during BAQS-Met 2007, Atmospheric Chemistry and Physics, 11, 7955-7973, 10.5194/acp-11-7955-2011, 2011.

Stockwell, W. R., Middleton, P., Chang, J. S., and Tang, X. Y.: The 2nd Generation Regional Acid Deposition Model Chemical Mechanism for Regional Air-Quality Modeling, J Geophys Res-Atmos, 95, 16343-16367, 1990.

Van Dingenen, R., Dentener, F. J., Raes, F., Krol, M. C., Emberson, L., and Cofala, J.: The global impact of ozone on agricultural crop yields under current and future air quality legislation, Atmospheric Environment, 43, 604-618, 10.1016/j.atmosenv.2008.10.033, 2009.

Wang, T., Xue, L., Brimblecombe, P., Lam, Y. F., Li, L., and Zhang, L.: Ozone pollution in China: A review of concentrations, meteorological influences, chemical precursors, and effects, Sci Total Environ, 575, 1582-1596, 10.1016/j.scitotenv.2016.10.081, 2017.

Wang, X., Chen, F., Wu, Z., Zhang, M., Tewari, M., Guenther, A., and Wiedinmyer, C.: Impacts of weather conditions modified by urban expansion on surface ozone: Comparison between the Pearl River Delta and Yangtze River Delta regions, Advances in Atmospheric Sciences, 26, 962-972, 10.1007/s00376-009-8001-2, 2009.

Wang, Y., Gao, W., Wang, S., Song, T., Gong, Z., Ji, D., Wang, L., Liu, Z., Tang, G., Huo, Y., Tian, S., Li, J., Li, M., Yang, Y., Chu, B., Petäjä, T., Kerminen, V.-M., He, H., Hao, J., Kulmala, M., Wang, Y., and Zhang, Y.: Contrasting trends of $PM_{2.5}$ and surface-ozone concentrations in China from 2013 to 2017, National Science Review, 7, 1331-1339, 10.1093/nsr/nwaa032, 2020.

Wentworth, G. R., Murphy, J. G., and Sills, D. M. L.: Impact of lake breezes on ozone and nitrogen oxides in the Greater Toronto Area, Atmospheric Environment, 109, 52-60, 10.1016/j.atmosenv.2015.03.002, 2015.

Worden, H. M., Bowman, K. W., Worden, J. R., Eldering, A., and Beer, R.: Satellite measurements of the clear-sky greenhouse effect from tropospheric ozone, Nature Geoscience, 1, 305-308, 2008.

~~Xie, M., Zhu, K., Wang, T., Yang, H., Zhuang, B., Li, S., Li, M., Zhu, X., and Ouyang, Y.: Application of photochemical indicators to evaluate ozone nonlinear chemistry and pollution control countermeasure in China, Atmospheric Environment, 99, 466-473, 10.1016/j.atmosenv.2014.10.013, 2014.~~

Xie, M., Liao, J., Wang, T., Zhu, K., Zhuang, B., Han, Y., Li, M., and Li, S.: Modeling of the anthropogenic heat flux and its effect on regional meteorology and air quality over the Yangtze River Delta region, China, Atmospheric Chemistry and Physics, 16, 6071-6089, 10.5194/acp-16-6071-2016, 2016a.

~~Xie, M., Zhu, K., Wang, T., Feng, W., Gao, D., Li, M., Li, S., Zhuang, B., Han, Y., Chen, P., and Liao, J.: Changes in regional meteorology induced by anthropogenic heat and their impacts on air quality in South China, Atmospheric Chemistry and Physics, 16, 15011-15031, 10.5194/acp-16-15011-2016, 2016b.~~

Xie, M., Shu, L., Wang, T.-j., Liu, Q., Gao, D., Li, S., Zhuang, B.-l., Han, Y., Li, M.-m., and Chen, P.-l.: Natural emissions under future climate condition and their effects on surface ozone in the Yangtze River Delta region, China, Atmospheric Environment, 150, 162-180, 10.1016/j.atmosenv.2016.11.053, 2017.

Xie, M., Zhu, K., Wang, T., Feng, W., Gao, D., Li, M., Li, S., Zhuang, B., Han, Y., Chen, P., and Liao, J.: Changes in regional meteorology induced by anthropogenic heat and their impacts on air quality in South China, Atmospheric Chemistry and Physics, 16, 15011-15031, 10.5194/acp-16-15011-2016, 2016b.

Xie, M., Zhu, K., Wang, T., Yang, H., Zhuang, B., Li, S., Li, M., Zhu, X., and Ouyang, Y.: Application of photochemical indicators to evaluate ozone nonlinear chemistry and pollution control countermeasure in China, Atmospheric Environment, 99, 466-473, 10.1016/j.atmosenv.2014.10.013, 2014.

You, C., Fung, J. C. H., and Tse, W. P.: Response of the Sea Breeze to Urbanization in the Pearl River Delta Region, Journal of Applied Meteorology and Climatology, 58, 1449-1463, 2019.

Young, P. J., Archibald, A. T., Bowman, K. W., Lamarque, J. F., Naik, V., Stevenson, D. S., Tilmes, S., Voulgarakis, A., Wild, O., Bergmann, D., Cameron-Smith, P., Cionni, I., Collins, W. J., Dalsøren, S. B., Doherty, R. M., Eyring, V., Faluvegi, G., Horowitz, L. W., Josse, B., Lee, Y. H., MacKenzie, I. A., Nagashima, T., Plummer, D. A., Righi, M., Rumbold, S. T., Skeie, R. B., Shindell, D. T., Strode, S. A., Sudo, K., Szopa, S., and Zeng, G.: Pre-industrial to end 21st century projections of tropospheric ozone from the Atmospheric Chemistry and Climate Model Intercomparison Project (ACCMIP), Atmospheric Chemistry and Physics, 13, 2063-2090, 10.5194/acp-13-2063-2013, 2013.

Yu, M., Carmichael, G. R., Zhu, T., and Cheng, Y.: Sensitivity of predicted pollutant levels to urbanization in China, Atmospheric Environment, 60, 544-554, 10.1016/j.atmosenv.2012.06.075, 2012.

Zhan, C.-c., Xie, M., Fang, D.-x., Wang, T.-j., Wu, Z., Lu, H., Li, M.-m., Chen, P.-l., Zhuang, B.-l., Li, S., Zhang, Z.-q., Gao, D., Ren, J.-y., and Zhao, M.: Synoptic weather patterns and their impacts on regional particle pollution in the city cluster of the Sichuan Basin, China, Atmospheric Environment, 208, 34-47, 10.1016/j.atmosenv.2019.03.033, 2019.

Zhan, C., Xie, M., Huang, C., Liu, J., Wang, T., Xu, M., Ma, C., Yu, J., Jiao, Y., Li, M., Li, S., Zhuang, B., Zhao, M., and Nie, D.: Ozone affected by a succession of four landfall typhoons in the Yangtze River Delta, China: major processes and health impacts, Atmospheric Chemistry and Physics, 20, 13781-13799, 10.5194/acp-20-13781-2020, 2020.

Zhan, C., Xie, M., Liu, J., Wang, T., Xu, M., Chen, B., Li, S., Zhuang, B., and Li, M.: Surface Ozone in the Yangtze River Delta, China: A Synthesis of Basic Features, Meteorological Driving Factors, and Health Impacts, Journal of Geophysical Research: Atmospheres, 126, 10.1029/2020jd033600, 2021.

Zhan, C.-c., Xie, M., Fang, D.-x., Wang, T.-j., Wu, Z., Lu, H., Li, M.-m., Chen, P.-l., Zhuang, B.-l., Li, S., Zhang, Z.-q., Gao, D., Ren, J.-y., and Zhao, M.: Synoptic weather patterns and their impacts on regional particle pollution in the city cluster of the Sichuan Basin, China, Atmospheric Environment, 208, 34-47, 10.1016/j.atmosenv.2019.03.033, 2019.

Zhang, N., Zhu, L., and Zhu, Y.: Urban heat island and boundary layer structures under hot weather synoptic conditions: A case study of Suzhou City, China, Advances in Atmospheric Sciences, 28, 855-865, 10.1007/s00376-010-0040-1, 2011.

Zhang, H., Wang, Y., Hu, J., Ying, Q., and Hu, X. M.: Relationships between meteorological parameters and criteria air pollutants in three megacities in China, Environ Res, 140, 242-254, 10.1016/j.envres.2015.04.004, 2015.

Zhu, B., Kang, H., Zhu, T., Su, J., Hou, X., and Gao, J.: Impact of Shanghai urban land surface forcing on downstream city ozone chemistry, Journal of Geophysical Research: Atmospheres, 120, 4340-4351, 10.1002/2014jd022859, 2015.